

HectD1 Controls Hematopoietic Stem Cell Regeneration by Coordinating Ribosome Assembly and Protein Synthesis

Kaosheng Lv,^{1,2} Chujie Gong,^{1,2} Charles Antony,³ Xu Han,^{1,2} Jian-Gang Ren,^{1,2} Ryan
Donaghy,^{1,2} Ying Cheng,^{1,2,4} Simone Pellegrino,^{5,6,7} Alan J. Warren,^{5,6,7} Vikram R. Paralkar,³
and Wei Tong^{1,2,8,*}

¹ Division of Hematology, Children's Hospital of Philadelphia, Philadelphia, PA 19104

² Division of Pediatrics, Perelman School of Medicine at the University of Pennsylvania,
Philadelphia, PA 19104

³ Division of Hematology-Oncology, Department of Medicine, Perelman School of Medicine
at the University of Pennsylvania, Philadelphia, PA 19104

⁴ Present address: Center for Mitochondrial Biology and Medicine, The Key Laboratory of
Biomedical Information Engineering of Ministry of Education, School of Life Science and
Technology, Xi'an Jiaotong University, Xi'an, China. 710049

⁵ Cambridge Institute for Medical Research, Cambridge, United Kingdom

⁶ Department of Haematology, University of Cambridge, Cambridge, United Kingdom

⁷ Wellcome Trust–Medical Research Council Stem Cell Institute, University of Cambridge,
Cambridge, United Kingdom

⁸ Lead Contact

* Correspondence author: tongw@chop.edu

Keywords

Hematopoietic stem cells (HSCs), ubiquitin, signaling, ribosome biogenesis, protein synthesis,
ribosome assembly.

Running title: HectD1 controls ribosome assembly in HSCs

Summary

Impaired ribosome function is the underlying etiology in a group of bone marrow failure syndromes called ribosomopathies. However, how ribosomes are regulated remains poorly understood, as are approaches to restore hematopoietic stem cell (HSC) function attributable to defective ribosome biogenesis. Here we reveal a role for the E3 ubiquitin ligase HectD1 in regulating HSC function via ribosome assembly and protein translation. *Hectd1*-deficient HSCs exhibit a striking defect in transplantation ability and ex vivo maintenance, concomitant with a reduced protein synthesis and growth rate under stress conditions. Mechanistically, HectD1 ubiquitinates and degrades ZNF622, an assembly factor for the ribosomal 60S subunit. *HectD1* loss led to an accumulation of ZNF622 and the anti-association factor eIF6 on the 60S, resulting in 60S/40S joining defects. Importantly, *Znf622* depletion in *Hectd1*-deficient HSCs restored ribosomal subunit joining, protein synthesis, and HSC reconstitution capacity. These findings highlight the importance of ubiquitin-coordinated ribosome assembly in HSC regeneration.

Introduction

At the steady-state, protein synthesis rate is low in adult hematopoietic stem cells (HSCs) as compared with committed progenitors or differentiated cells (Signer et al., 2014). Tightly-regulated protein synthesis rate is critical for HSC maintenance and function (Signer et al., 2014; Signer et al., 2016). HSC expansion under regenerative or stress conditions demands increased ribosome biogenesis and protein synthesis. Appropriate ribosome biogenesis and assembly ensures the translation efficiency and fidelity of proteins, which are important for normal development as well as prevention of cancer. Mutations in ribosomal proteins and gene products affecting ribosome biogenesis and protein synthesis are associated with human diseases marked by hematopoietic dysfunction (Sulima et al., 2017). However, how ribosome assembly is regulated in HSCs remains poorly understood, as is its contribution to hematopoietic diseases.

The biogenesis of the two ribosomal subunits 40S and 60S occurs largely in the nucleus; upon nuclear export, they separately undergo final stages of maturation in the cytoplasm that are regulated by distinct assembly factors and incorporation of the last few cytoplasmic ribosome proteins (de la Cruz et al., 2015). These assembly factors proofread and protect key functional sites on the ribosome and prevent premature joining of 60S and 40S subunits, to ensure regulated formation of functional 80S monosomes and appropriate translation (Klinge and Woolford, 2019). “Ribosomopathies” are characterized by a group of inherited bone marrow failure (BMF) syndromes with impaired ribosome function. Individuals with “ribosomopathies” are deficient in HSCs or specific lineages of blood formation, and yet are predisposed to elevated leukemia and cancer risks (Ruggero and Shimamura, 2014). One such example is Shwachman-Diamond syndrome (SDS), that is etiologically linked to ribosome dysfunction arising from mutations of ribosome assembly factors (Warren, 2018; Woloszynek et al., 2004). Germline mutations in three different genes (*SBDS*, *DNAJC21*, and *EFL1*) involved in the 60S maturation and assembly all

cause SDS (Boocock et al., 2003; Dhanraj et al., 2017; Tan et al., 2019; Tummala et al., 2016; Woloszynek et al., 2004), implying that HSCs are especially sensitive to perturbations in ribosome assembly. These mutations result in ribosomal subunit joining defects and decreased protein synthesis rate (Finch et al., 2011; Menne et al., 2007; Tan et al., 2019; Wong et al., 2011). The question of how ribosomal abnormalities cause marrow failure and cancer predisposition is therefore of fundamental biological and clinical interest. However, how assembly factors themselves are regulated and their impact on hematopoietic regeneration remain poorly understood.

HectD1, a member of HECT domain E3 ligases, plays an indispensable role in early embryogenesis. The HECT domain of HectD1 catalyzes the ubiquitination of its substrates to modulate protein stability, protein-protein interaction, and cellular localization. HectD1 has been reported to regulate various biological processes, including signaling transduction, gene transcription, development, and lipid homeostasis (Aleidi et al., 2018; Li et al., 2015; Sarkar and Zohn, 2012; Sugrue et al., 2019; Tran et al., 2013). Here, we identify HectD1 as a critical determinant of HSC function via its direct ubiquitination of ribosomal assembly factor. This discovery provides an important new facet to our understanding of ubiquitin-coordinated ribosomal assembly in stem cell biology.

Results

Generation of a conditional *Hectd1* knockout mice in hematopoietic cells.

Hectd1 germline knockout (KO) leads to mouse embryonic lethality due to defects in neural tube closure and impaired placenta development (D'Alonzo et al., 2019; Sarkar et al., 2014; Zohn et al., 2007). To explore a potential role for HectD1 in hematopoiesis, we studied a conditional *Hectd1* knockout (cKO) mouse model (Figure S1A). The floxed alleles of *Hectd1* that target exon 3 (*Hectd1^{flf}*) were crossed with *Vav-cre* transgenic mice, in which the Cre recombinase is under the

control of the *Vav* promoter to allow pan-hematopoietic excision of *Hectd1* in all hematopoietic cells (*Hectd1^{ff;Vav}*). Deletion of exon 3 is predicted to generate an early stop codon in exon 4, thus producing a non-functional 50 amino acid truncated protein. To evaluate deletion efficiency, we plated bone marrow (BM) cells from *Hectd1^{ff}* and *Hectd1^{ff;Vav}* mice into semisolid methylcellulose culture and confirmed a nearly 100% deletion efficiency by genotyping individual colonies (Figure S1B). Quantitative PCR analysis (qRT-PCR) demonstrated the specific targeting of exon 3 of the *Hectd1* gene (Figures S1C and S1D). Moreover, HectD1 protein was undetectable in *Hectd1^{ff;Vav}* BM cells (Figure S1E). Together, these data suggest that *Hectd1* was efficiently and specifically deleted in all hematopoietic cells in our cKO mouse model.

***Hectd1* deficiency impairs HSC repopulation capacity and decreases functional HSC frequency**

To elucidate the impact of *Hectd1* loss on homeostatic hematopoiesis, we first investigated the hematological parameters in young adult mice. Complete blood count (CBC) analysis and flow cytometry of different lineages of blood cells from *Hectd1^{ff;Vav}* mice showed largely normal blood counts compared with their *Hectd1^{ff}* littermates (Figures S2A and S2B). Total BM cellularity and spleen weight were also indistinguishable from controls (Figures S2C and S2D). We then characterized the hematopoietic stem and progenitor cells (HSPCs) in the BM and spleen. *Hectd1^{ff;Vav}* mice showed comparable HSPC frequencies and numbers to those of *Hectd1^{ff}* controls (Figures S2E-S2H), ie, long-term stem cells (LT-HSCs, Lin⁻Sca1⁺c-Kit⁺Flk2⁻CD150⁺CD48⁻), short-term stem cells (ST-HSCs, Flk2⁻CD150⁻CD48⁻ LSK), various multipotent progenitors (MPPs) (Lv et al., 2017). Furthermore, we observed no difference in the frequency and number of committed progenitor cells in the BM by flow cytometry (Figures S2I and S2J) or functional progenitors by colony-forming-cell (CFC) assay (Figure S2K). Interestingly, the spleen of *Hectd1^{ff;Vav}* mice displayed a significant increase in CMP and MEP progenitors (Figures S2L and

S2M), and accordingly, more CFU-E and CFU-GM colonies as compared to their *Hectd1^{ff}* littermates (Figure S2N). Moreover, the cell cycle status or apoptosis in HSCs and MPPs remained unchanged (Figures S2O-2Q). These observations indicate relatively normal hematopoiesis in young adult *Hectd1^{ff;Vav}* mice under homeostatic conditions.

To assess the consequences of *Hectd1* loss in HSC function *in vivo*, we performed competitive BM transplantation (BMT) assay by injecting 1×10^6 total BM cells from *Hectd1^{ff}* or *Hectd1^{ff;Vav}* donor mice (CD45.2) with an equal number of BM cells from competitor mice (CD45.1) into lethally irradiated recipients (CD45.1/CD45.2) (Figure 1A). Donor chimerism in the peripheral blood (PB) of the recipients was determined by flow cytometry every 4 weeks post-BMT. Of note, donor-derived cell percentages from *Hectd1^{ff;Vav}* mice were considerably decreased compared with control mice as early as 4 weeks, and exhibited a progressive decline over time (Figures 1B and 1C), indicating a defect in LT-repopulating HSCs. *Hectd1* loss did not affect lineage distribution in the transplanted recipients (Figures 1D and S3A-S3D). Importantly, the percentages of donor-derived HSPC populations from *Hectd1^{ff;Vav}* mice were substantially decreased in comparison to *Hectd1^{ff}* controls (Figure 1E), indicating a reduction in HSC reconstitution. To further examine the impact of *Hectd1* loss on HSC self-renewal, we performed secondary BMT by injecting 1×10^6 total BM cells from primary transplanted mice into secondary recipients. Defective reconstitution from *Hectd1^{ff;Vav}* mice was further exacerbated in secondary transplantation (Figure 1F). Thus, these data indicate that *Hectd1^{ff;Vav}* mice have inferior long-term BM repopulating HSCs with reduced self-renewal.

To functionally quantify HSC frequency, we next employed limiting dilution BMT (Figure 1G). A graded dose of BM cells from *Hectd1^{ff}* and *Hectd1^{ff;Vav}* mice mixed with a fixed number of competitor cells were transplanted into lethally irradiated recipient mice. 16 weeks after BMT,

mice with donor percentage higher than 1% were defined as “positive reconstitution” (Bersenev et al., 2008). We found that *Hectd1^{ff;Vav}* mice harbored a 4-fold reduction in functional HSC frequencies in the BM by ELDA analysis (extreme limiting dilution analysis) (Figure 1H) (Hu and Smyth, 2009). *Hectd1^{ff;Vav}* BM cells exhibited consistently reduced donor chimerisms in the recipients transplanted at all doses of donor cells (Figures 1I and S3E-S3G). Since HectD1 was reported to be involved in protein secretion and cell migration (Duhamel et al., 2018), we asked if *Hectd1* loss could affect BM niche or in a cell extrinsic manner. Therefore, we performed reciprocal BMT by injecting BM cells from wildtype mice (CD45.1) into *Hectd1^{ff}* or *Hectd1^{ff;Vav}* mice as recipients (CD45.2) (Figure S3H). Donor chimerism as well as lineage distribution in the PB and HSPCs in the BM were comparable among recipients of both genotypes (Figures S3I-S3K). Taken together, our data provide strong evidence that *Hectd1* insufficiency reduces frequencies of functional HSCs in the BM.

Hectd1* insufficiency diminishes HSC reconstituting activity *in vivo* and HSC growth *ex vivo

To further address if the decreased repopulation observed in total BM transplantation is due to intrinsic HSC properties, we purified LT-HSCs (LSK CD150⁺CD48⁻) from *Hectd1^{ff}* and *Hectd1^{ff;Vav}* mice by flow cytometric sorting and transplanted 100 HSCs into each lethally-irradiated recipient along with Sca1-depleted BM competitors (Figure 2A) (Balcerek et al., 2018). Our results demonstrated that *Hectd1*-deficient HSCs exhibited inferior reconstitution ability to that of control HSCs *in vivo* (Figure 2B). Importantly, donor-derived HSPCs in the BM of recipient mice transplanted with *Hectd1*-deficient HSCs were significantly reduced when compared with those from control HSCs (Figure 2C), indicating *Hectd1* insufficiency decreases intrinsic HSC activity.

We next analyzed the influence of HectD1 on the maintenance of HSC function upon *ex vivo* culture. Purified HSCs were cultured in media containing a combination of cytokines SCF, TPO,

FLT3L and IL6 for 12 days. The resultant cultured cells from 100 HSCs were transplanted (Figure 2A). Our data revealed that *Hectd1* insufficiency failed to maintain HSCs *ex vivo*, which was accompanied by a marked reduction in reconstituting capacity (9.0% cultured HSCs vs 57.8% fresh HSCs reconstitution at 16 weeks), while control HSCs showed comparable reconstitution after culture (92.0% cultured HSCs vs 82.0% fresh HSCs) (Figure 2D). Moreover, examination of donor-derived HSPCs in the BM of recipient mice revealed that *Hectd1*-deficient HSCs completely lost their stem cell identity in culture (Figure 2E). Importantly, we found that *Hectd1*-deficient HSCs had a visibly slower growth rate than control HSCs *ex vivo* as determined by enumeration of cell numbers, and this phenotype persisted irrespective of cytokines used in culture (Figures 2F-2I). Taken together, our data suggest that HectD1 is critical for HSC function *in vivo* and HSC growth *ex vivo*.

Since HectD1 is widely expressed in a range of hematopoietic cells, we asked if HectD1 is preferentially required for HSC function. To test this, we injected 500 purified HSCs (LSK CD150⁺CD48⁻) or 5000 MPPs/ hematopoietic progenitors (HPCs) (LSK CD150⁻CD48⁺) (Oguro et al., 2013; Pietras et al., 2015; Wilson et al., 2008) from *Hectd1*^{fl/fl} and *Hectd1*^{fl/fl;Vav} mice into each sub-lethally irradiated recipient and analyzed donor chimerism every week post-BMT (Figure 2J). Of note, our results showed that *Hectd1* deficiency markedly decreased HSC reconstitution ability, but not that of MPP/HPCs (Figures 2K, 2L and S3L, S3M), indicating that HectD1 plays a critical role in regulating HSC function.

HectD1 interacts with, ubiquitinates and regulates the stability of ZNF622

To study the mechanisms underlying the reduced growth of *Hectd1*-deficient HSPCs, we first evaluated known signaling pathways important for HSC function, ie, JAK-STAT, PI3K-AKT, MAPK-ERK, mTOR, GSK3 and β -catenin pathways (Figure S4A). However, none of these

signaling molecules were altered, except for a significant reduction of phospho-RPS6 (pRPS6) in both freshly isolated and cultured *Hectd1*-deficient LSK cells (Figures 3A and S4B).

To facilitate downstream biochemical studies, we resorted to cytokine-dependent human progenitor cell line, TF-1 cells. Using two different shRNAs to stably deplete *HECTD1* in human TF-1 cells, in comparison to Luciferase (Luc) control (Figure 3B), we observed a significant growth retardation in the presence of TPO or GM-CSF upon *HECTD1* knockdown (Figures 3C and 3D), consistent with findings from HSPCs (Figures 2F-2I). TF-1 cells also recapitulated the signaling defects observed in primary LSK cells, which is a reduction in RPS6 phosphorylation but not any other pathways we examined (Figures S4C-S4E). Thus, TF-1 cells appear to be a reliable and robust cell system for us to further dissect HectD1 functions.

Intriguingly, the reduction of pRPS6 seemed to be independent of mTOR pathway since p-mTOR, p4E-BP1, pS6K1 and a S6K1 substrate pZRF (Barilari et al., 2017) were not changed (Figures 3A and S4B). This led us to hypothesize that HectD1 might directly ubiquitinate RPS6 or regulate S6K1-RPS6 interaction as K63-ubiquitination is known to affect protein complex formation (Shembade and Harhaj, 2015). However, neither RPS6 ubiquitination nor the S6K1-RPS6 interaction was impacted by HectD1 E3 dead mutant C2579G (Mut) (Sarkar and Zohn, 2012) or *HECTD1* knockdown (Figures S4F-S4H), implying that HectD1 indirectly affects RPS6 phosphorylation. The phospho-RPS6 has been shown to control the RiBi- (ribosome biogenesis) gene transcriptional program (Chauvin et al., 2014). We found that *Hectd1*-deficient HSCs did not exhibit changes in either total RNA level that is predominantly rRNAs or the mRNA level of the RiBi genes relatively to that of control cells (Figures S4I and S4J).

In an attempt to explore the molecular mechanism underlying the important role for *Hectd1* in HSCs in a comprehensive and unbiased manner, we set out to identify HectD1 substrates by affinity purification of HectD1 interacting protein complex using mass spectrometry (MS). We transfected HA-tagged HectD1 or vector alone into HEK293T cells. HectdD1-interacting proteins were immunoprecipitated (IP) using anti-HA agarose beads, followed by HA peptide affinity elution. Glycine elution after HA elution detected very few bound proteins, and the non-specific proteins remained associated with the agarose beads upon boiling in SDS loading buffer, indicating the specificity and robustness of HA-affinity purification (Figure 3E). We thus subjected the HA eluates to MS analysis along with vector control. Triplicates of IP-MS were performed and results were evaluated using the CRAPome (Contaminant Repository for Affinity Purification) analysis (Mellacheruvu et al., 2013). We ranked and selected the potential interacting proteins with the cutoff of SAINT (Significance Analysis of INteractome) score ≥ 0.5 and fold change (FC) ≥ 3 (Figure 3F). Gene ontology (GO) analysis revealed a high enrichment of ribosome/translation-related proteins and proteasome proteins (Figure S5A and Supplementary Table S1), which is in agreement with the role of HectD1 as an E3 ubiquitin ligase and regulator of cell growth. Additionally, it suggested a potential role for HectD1 in ribosomes and protein synthesis.

Among the top hits, we focused on ZNF622 protein, given the critical role of its yeast homolog Rei1 in ribosome biogenesis (Greber et al., 2016; Meyer et al., 2010). The interaction between HectD1 and ZNF622 was first confirmed in Flag-ZNF622 reconstituted TF-1 cells by co-IP (Figure 3G). Next, we generated a series of deletion mutants of HectD1 and ZNF622, and transfected them into 293T cells, followed by IP/WB analysis to map the responsible domain(s) for their interaction. Our data showed that Hectd1 interacted with ZNF622 regardless of its E3 activity as both HA-Hectd1 WT, and E3 dead mutant C2579G (Mut), but not vector control could pull down endogenous ZNF622. We also found that the Sad1/UNC domain of HectD1 is

responsible for its interaction with ZNF622 (Figures S5B and S5C). Furthermore, deletion of either ZnF2 domain or the first linker region (LR1) located in the N-terminus of ZNF622 completely abolished its interaction with HectD1 (Figures S5D and S5E). Interestingly, cryo-EM analysis has revealed that these two regions of Rei1 are located outside of the polypeptide tunnel (Greber et al., 2016; Kargas et al., 2019), rendering it accessible to HectD1 interaction.

Next, we asked if HectD1 regulates ZNF622 ubiquitination and protein stability. We found that *Hectd1* deficiency increased ZNF622 protein, but not mRNA levels in LSK cells (Figures 3H-3J). Consistently, ZNF622 protein but not mRNA level was increased in *HECTD1*-depleted TF-1 cells (Figures 3K, 3L and S5F). Importantly, the half-life of ZNF622 proteins was significantly prolonged in *HECTD1*-depleted TF-1 cells in the presence of cycloheximide (CHX) that blocks nascent protein synthesis (Figures 3K and 3L). Next, we analyzed ZNF622 ubiquitination status impacted by HectD1 using Nickel-beads (Ni-NTA) pulldown of His-tagged Ub under denatured conditions to capture direct Ub-conjugation in ZNF622 proteins while reducing the detection of its associated proteins. Our data demonstrated that ZNF622 was robustly ubiquitinated by WT HectD1, but not the C2579G mutant. Moreover, consistent with the notion of HectD1 being an E3 ligase for lysine⁶³-polyubiquitination (K63-Ub) (Sarkar and Zohn, 2012), K63R, but not K48R Ub mutant, abolished ZNF622 ubiquitination (Figure 3M), further demonstrating that ZNF622 is a direct substrate of HectD1. Taken together, our data suggest that HectD1 interacts with, ubiquitinates and regulates the stability of ZNF622.

***Hectd1* insufficiency decreases HSPC proliferation and global translation rates upon stress**

The HectD1 IP-MS data and the interaction between HectD1-ZNF622 promoted us to investigate a potential role for HectD1 in protein synthesis and ribosome biology. To test this, we performed *in vivo* OP-puro (O-propargyl Puromycin) assay in primary adult *Hectd1^{ff}* and *Hectd1^{ff;Vav}* mice

to evaluate protein synthesis rate (Liu et al., 2012). We found that HSCs exhibited a lower protein synthesis rate than restricted progenitors and mature hematopoietic cells (Figures S5G and S5H), consistent with the previous report (Signer et al., 2014). However, *Hectd1* insufficiency did not affect protein synthesis rates in any of the hematopoietic cell subsets at the steady state (Figure S5H).

Our data showed that *Hectd1* deficiency does not affect phenotypic HSC number in the steady state (Figure S2G), but dramatically decreases functional HSCs in the transplantation assay or *ex vivo* culture, both of which conditions force HSCs to proliferate (Figures 1 and 2). Thus, we investigated if HectD1 is critical for HSC proliferation *in vivo* under stress conditions. We subjected the mice to two different types of stress. We first challenged *Hectd1^{ff/ff}* and *Hectd1^{ff/ff};Vav* mice with cytotoxic drug 5-fluorouracil (5-FU), which depletes cycling hematopoietic cells and drives primitive HSCs to regenerate. At day 10 after 5-FU administration, *Hectd1^{ff/ff};Vav* mice exhibited a pronounced reduction in BM HSC and MPP numbers in comparison to the control mice (Figure 4A). Notably, both *Hectd1* deficient HSCs and MPPs showed reduced protein synthesis rate using the OP-Puro assay (Figures 4B and 4C), which correlated with their slower cycling status than the controls as determined by BrdU incorporation (Figure 4D). We did not observe elevated cell death under 5-FU stress (Figure S5I). To consolidate the conclusion of HectD1 function under stress conditions, we subjected mice to cyclophosphamide treatment followed by two daily doses of G-CSF to induce HSPC proliferation (Morrison et al., 1997). In agreement, our data revealed lower HSC and MPP numbers (Figure 4E), slower cell cycle kinetics, as well as decreased protein synthesis rate in *Hectd1^{ff/ff};Vav* mice in comparison to the controls (Figures 4F-4H).

Next, we examined OP-Puro incorporation in *ex vivo* cultured LSK cells, which were also undergoing proliferative stress. *Hectd1*-deficient cells displayed a decrease in global translation rate by >20% when compared to control LSKs (Figures 4I and 4J). Consistently, *Hectd1*-deficient BM progenitors were hypersensitive to puromycin, an inhibitor of translation elongation (Figure 4K). Of note, this observed translation defect in both primary LSK cells and TF-1 cells was independent of eIF2 α or 4E-BP1 phosphorylation, two key regulators of translation initiation (Figures S4B-S4E) (Holcik and Sonenberg, 2005). Taken together, we demonstrate that HectD1 plays a critical role in HSPC proliferation and protein synthesis under hematopoietic stress.

***Hectd1* deficiency disrupts ZNF622-mediated 60S ribosome maturation and 60S/40S subunit joining**

To dissect molecular mechanisms by which HectD1 regulates ribosome assembly and protein translation, we examined whether HectD1 affects ribosome composition by polysome profiling assay. Cell lysates of equal RNA content were fractionated in a sucrose gradient, followed by recording of the ultraviolet (UV) absorbance of each fraction. *Hectd1*-null LSK cells displayed an increased 60S content but decreased 80S monosome and polysome, while 40S remained unchanged (Figure 5A). This phenotype was also observed in *HECTD1*-depleted TF-1 cells (Figure 5B). These data indicated a previously-unrecognized role for HectD1 in regulating ribosome assembly and proper global translation.

During ribosome biogenesis, subunits are exported to the cytoplasm as pre-60S and pre-40S complexes that must undergo final maturation involving sequential addition and release of a series of proteins to form mature 60S and 40S subunits (de la Cruz et al., 2015; Kargas et al., 2019). In yeast, ZNF622 homolog Rei1, stabilizes Arx1 (human PA2G4) association with pre-60S (Greber et al., 2012). Jjj1 (human DNAJC21) is required for the release of Rei1-Arx1 complex and the

completion of polypeptide exit tunnel (PET) maturation (Lo et al., 2010; Meyer et al., 2010). Failure of Rei1/Arx1 dissociation from pre-60S particles precludes downstream assembly events, including the anti-association factor eIF6 release from pre-60S, which is a crucial step for 40S joining to form a functional ribosome. Thus, we sought to test if the elevated ZNF622 level in *HECTD1*-depleted cells would affect 60S maturation. Fractions of shLuc or sh*HECTD1* TF-1 cells from the sucrose gradient were collected and examined by WB. The results showed that HECTD1 was predominantly located in the cytosol, with a small fraction detected in free ribosome subunits (Figure 5C). Notably, ZNF622 was predominantly associated with the 60S, and *HECTD1* depletion resulted in a marked accumulation of ZNF622 in the 60S (Figures 5C and 5D). In contrast, the 40S protein Nob1 remained unchanged. Moreover, the ZNF622 binding partner PA2G4 and downstream eIF6 were markedly increased in the 60S, indicating an abnormal 60S ribosome formation (Figures 5C and 5D). Interestingly, the ribosome biogenesis factor for the maturation of the polypeptidyl transferase center (PTC), NMD3, was unchanged (Figures 5C and S6), indicating that the regulation of PET and PTC may be uncoupled. Besides the association and release of assembly factors, the cytoplasmic maturation of pre-60S subunit involves the concomitant incorporation of cytoplasmic ribosome proteins (de la Cruz et al., 2015; Kargas et al., 2019). Consistent with this notion, we found impaired incorporation of cytoplasmic RPL24 in the polysomes of *HECTD1*-depleted cells (Figures 5C and 5D), whereas other core RPL proteins that were pre-assembled in the nucleus, such as RPL11 and RPL23A, were unaffected (Figures 5C and S6). Of note, we observed a reduced pRPS6 level but not total RPS6 in *HECTD1* deficient cells when compared to the controls (Figures 5C and S6). Together, these data suggest that increased ZNF622 proteins upon *HECTD1* loss leads to a defective 60S maturation or activation of a translational quality control pathway arising from a block in the release of PA2G4 and eIF6, reduced joining of 60S and 40S, thereby resulting in reduced 80S and polysomes.

To gain further insight into the role for HectD1 in the regulation of ZNF622 in 60S formation and 60S/40S subunit joining, we assessed if depletion of ZNF622 could rescue the ribosome defects observed upon *HECTD1* loss. We compared the polysome profiling and eIF6 retention in the 60S of shLuc control, *HECTD1* single and *HECTD1*; *ZNF622* double knockdown (DKD) TF-1 cells (Figure 5E). Our data showed that knockdown of ZNF622 in *HECTD1*-deficient cells restored ribosome composition as well as eIF6 release to normal levels (Figures 5F-5H). Furthermore, we performed ribosome dissociation/reassociation assay with these cell lines to directly interrogate 60S/40S subunit joining (Burwick et al., 2012). 80S monosomes and polysomes were first dissociated into 40S and 60S subunits under low Mg^{2+} conditions, and the total amount of 40S and 60S was comparable among these three cell lines (Figures 5I and 5J). We subsequently added back Mg^{2+} allow 40S and 60S subunits to reassociate. *HECTD1* depletion reduced ribosomal reassociation. Importantly, this disruption in ribosomal reassociation was reversed by ZNF622 knockdown (Figures 5I and 5J). Taken together, these results provide direct evidence that HectD1 plays an essential role in controlling 60S/40S subunit joining and translational control by regulating ZNF622.

ZNF622 depletion restores protein translation and HSC transplantation activity induced by *Hectd1* loss

We reasoned that if the compromised translation rate observed in *Hectd1*-deficient cells was owing to the elevated ZNF622 level and ZNF622-mediated ribosome defects, attenuation of ZNF622 expression would be able to rescue this phenotype. To test this hypothesis, we knocked down ZNF622 with shRNA in *Luc*- or *HECTD1*-depleted TF-1 cells (Figure 6A). Strikingly, ZNF622-depletion fully restored protein synthesis rate to normal levels in *HECTD1*-depleted cells, while it did not significantly affect the translation rate in control cells as examined by the OP-Puro assay

(Figure 6B). Of note, *ZNF622* downregulation restored pRPS6 level in *HECTD1*-depleted cells that was independent of mTOR (Figures 6A and S6G).

We next asked if the aberrant accumulation of ZNF622 accounts for the perturbed HSC activity owing to *Hectd1* deficiency. To functionally test this, we depleted *Znf622* in *Hectd1*-null HSCs and examined their reconstitution ability. We first generated two efficient shRNAs against mouse *Znf622* (sh*Znf622*#1 and #2) with #1 shRNA being the most robust (Figure 6C). Subsequently, LSK cells were purified from *Hectd1^{ff/ff};Vav* mice and infected with lentivirus expressing sh*Luc* or two shRNAs to *Znf622* with mCherry as a fluorescent marker. We injected 250k lentivirally-infected LSKs into each recipient with 500k *Sca1*-depleted competitor BM cells to ensure high donor reconstitution and recipient survival (Figure 6D) (Jiang et al., 2012). Both *Znf622* shRNAs increased the reconstitution of *Hectd1*-deficient HSCs in the peripheral blood (PB) of the recipient mice (Figure 6E). Importantly, mice transplanted with LSKs depleted of *Znf622* had a significantly higher proportion of mCherry⁺ cells in the BM HSCs and MPPs than those with sh*Luc* (Figure 6F). Therefore, the restored donor chimerism observed in the PB was resulted from HSC restoration.

We next examined if the rescue effect of *Znf622* downregulation was specific to *Hectd1*-null background. LSKs from both *Hectd1^{ff/ff}* and *Hectd1^{ff/ff};Vav* mice were sorted and infected with lentivirus expressing sh*Luc* or sh*Znf622*#1 followed by BMT. While control HSC reconstitution in the PB was not significantly affected by *Znf622* knockdown, *Hectd1*-deficient HSC reconstitution ability was significantly rescued (Figure 6G), and importantly, that was attributed to restored HSPC populations (Figure 6H). Strikingly, mCherry⁺ donor chimerism in the PB of secondary recipients further validated the HSC promoting effect of *Znf622* knockdown as the reconstitution ability of *Znf622*-depleted *Hectd1*-null cells was significantly elevated in comparison to control cells (Figure 6I). To summarize, these data support a working model that

ZNF622 is an important functional mediator of HectD1 function in regulating ribosome assembly and protein translation efficiency, as well as HSC regeneration.

Discussion

Tightly-regulated protein synthesis rate is critical for HSC maintenance and function, as only a 30% decrease (using *Rpl24^{Bst/+}* mice, where ribosome protein Rpl24 is partially depleted) or increase (cKO of *Pten* or *4E-BP1/2* mice) in protein synthesis is sufficient to impair HSC proliferation and self-renewal (Signer et al., 2014; Signer et al., 2016). Here we identified a critical role for ubiquitin-dependent regulation of ribosome assembly by HectD1 to meet the increased protein demands during HSC regeneration *in vivo* and *ex vivo*.

We demonstrate that HectD1 is required for HSC but not progenitor cell expansion *in vivo*, pointing to that balanced protein synthesis is essential for HSC function. Interestingly, HectD1 is dispensable for HSC development during homeostasis, but is critical for HSC regeneration under proliferative stress. Of note, HectD1 is found indispensable in all hematopoietic stress conditions we tested, such as *in vivo* transplant settings, *ex vivo* expansion under cytokines, as well as genotoxic stress 5-FU or cyclophosphamide/GCSF-induced HSPC proliferation. The extraordinary demands for HSPC growth and proliferation in these conditions require increased global protein production, thereby coordinated ribosome production. The data in this report suggest that HectD1 controls ribosome assembly and protein synthesis rate during HSC regeneration by regulating 60S assembly factor ZNF622. Of note, we cannot exclude the possibility that HectD1 also regulates protein synthesis and cell cycle in some, and potentially many, hematopoietic progenitors after injury.

Impaired ribosome function arising from genetic aberrations of RP proteins or assembly factors causes a group of human disorders known as “ribosomopathies”, such as SDS. 90% of SDS patients harbor mutations in the *SBDS* gene, which functions with the GTPase EFL1 to facilitate the removal of anti-association factor eIF6 from pre-60S ribosomal subunits to allow the assembly of 40S and 60S into functional monosomes (Finch et al., 2011; Menne et al., 2007; Warren, 2018; Weis et al., 2015). In addition, biallelic mutations in DNAJC21, a maturation factor for the PET, cause abnormal accumulation of PA2G4 and eIF6 in pre-60S ribosomal subunits and reduce 60S and 40S joining, eliciting an SDS-like phenotype (Dhanraj et al., 2017; Tummala et al., 2016). It is noteworthy that DNAJC21 assists the release of ZNF622-PA2G4 from pre-60S, allowing for the progression of downstream maturation steps. Thus, our data suggest that *Hectd1* deficiency recapitulates both the molecular ribosomal abnormalities and the phenotypic perturbations in HSCs, reminiscent of SDS. We found that depletion of *ZNF622* in *HECTD1*-deficient cells rescues ribosome composition as well as eIF6 release to normal levels, thereby restoring 60S/40S subunit joining and protein translation. Notably, it also supports the idea that *ZNF622* influences the affinity of eIF6 for the ribosome, thereby serving as a quality control step to ensure proper ribosome assembly. More importantly, we demonstrate that downregulation of *Znf622* rescues HSC reconstitution capacity in *Hectd1*-null mice, implicating *ZNF622* inhibition as a potential therapeutic strategy for the treatment of BMF disease with defective ribosomes.

It is important to point out that structure-function studies of ribosome biogenesis and assembly factors have been most examined in yeast and prokaryotes. Our work provides significant biochemical and functional insight into the critical biogenesis factors of human and mouse ribosomes. Structural analysis of the yeast homolog of *ZNF622*, *Rei1*, revealed that the *Rei1* C-terminus is deeply inserted into the 60S PET, which is essential for the proofreading of PET maturation and subsequent *Arx1* (yeast PA2G4) liberation and eIF6 eviction steps (Greber et al.,

2016). Our data in human hematopoietic cells demonstrate that accumulated ZNF622 in pre-60S blocks PA2G4 removal and efficient ribosome maturation, in accordance with the function of Rei1 in Arx1 release in yeast cells (Meyer et al., 2010). An alternative but not mutually-exclusive explanation points to a subunit joining and translation defect rather than a biogenesis defect upon *HECTD1* loss, since the amount of total 40S and 60S was unaffected. In the absence of *HECTD1*, ZNF622 abnormally accumulates in the pre-60S and/or rebinds to mature 60S to block 60S/40S joining via ZNF622-associated eIF6. A role for ZNF622 and eIF6 in ribosomal stress and translational quality control has been suggested in a whole-genome CRISPRi screen in human chronic myeloid leukemia (CML) cell line. This study revealed that depletion of *ZNF622* or *eIF6* restores cell fitness and cell growth in the presence of PF8503, a translational inhibitor that binds to the PET and inhibits the translation of selective proteins and suppresses cell proliferation (Liaud et al., 2019). Hence, our work may uncover a ribosome quality control pathway that is critical for HSPCs during regenerative or proliferative stress. Under this circumstance, high demand for protein synthesis increases the need for ribosome quality control, where *HECTD1* activity controls ZNF622 and eIF6-mediated ribosome assembly and protein translation efficiency.

In yeast, Rei1-Arx1 departure from 60S coincides with the exchange for the Rei1 family member Reh1 in the PET that persists in the later stages of cytoplasmic maturation process (Kargas et al., 2019; Ma et al., 2017). This finding is in striking contrast to those reported in yeast, in which dual knockout of Rei1 and Reh1 severely constrains yeast cell growth (Greber et al., 2016). Therefore, it is possible that ZNF622 exerts a distinct function from its yeast homologs. The N-terminus of Rei1 contacts RPL24 on the surface of the 60S ribosome (Greber et al., 2016) and directly interacts with eIF6 (Kargas et al., 2019). ZNF622 may regulate eIF6 release through its direct interaction with eIF6, or indirectly through RPL24. In agreement, we demonstrate that increased ZNF622 protein level coincides with an accumulation of eIF6 in the 60S subunit of *HECTD1*-depleted cells

and depletion of ZNF622 reduces eIF6 association in the 60S. Of note, RPL24 is essential for the formation of 60S-40S inter-subunit bridges, one of which depends on the direct interaction between RPL24 and RPS6 (Kisly et al., 2019). Our data raise the possibility that RPS6 phosphorylation serves as a feedback regulation in the 40S subunit when the 60S large subunit encounters stress, as we observed a correlation between pRPS6 and 60S maturation and protein synthesis in this context. Nonetheless, the intricate regulation between different ribosome subunits and monosomes/polysomes mandates future investigations.

Taken together, we reveal a ubiquitin-dependent control of ribosome assembly and protein synthesis that is essential to HSC activity and regeneration, highlighting the importance of ribosome assembly factors in HSC function. Importantly, we demonstrate that *Znf622* depletion restores 60S ribosome maturation, ribosome assembly, protein synthesis and HSC activity in the context of *Hectd1* deficiency. This finding establishes an *in vivo* example of genetic suppression of HSC defects associated with dysfunctional ribosomes. Hence, it will likely enhance our understanding of the pathogenesis and therapeutic strategies for ribosomopathies.

Limitations of the Study

Our work demonstrates that the E3 ubiquitin ligase HectD1 plays an important role in HSC regeneration by ubiquitin-dependent regulation of ribosome assembly via ZNF622. While our study provides strong evidence for HectD1/ZNF622-mediated protein translation in HSPCs under stress conditions, it is unclear if they play a role in 60S ribosome biogenesis or quality control of stressed ribosomes. We also found that the level of phospho-RPS6 was dramatically decreased in *Hectd1*-deficient cells and this correlates with reduced protein synthesis rate and HSPC function. However, we do not understand the underlying mechanism or its relevance to ZNF622. Another limitation is that we immunoblotted and quantified the distribution of ribosomal proteins and

association factors in ribosomal fractions of a hematopoietic cell line TF-1 cells, but not in HSPCs due to their scarcity.

Acknowledgements

WT is supported by NIH grants R01DK127738 and R01HL095675, awards from Department of Defense, St. Baldrick's Foundation, Alex's Lemonade Research Foundation, and Basser Center for BRCA Research. VRP is supported by an NIH grant R35 GM138035. AJW is supported by a Specialist Programme from Blood Cancer UK (12048, to AJW), the UK Medical Research Council (MR/T012412/1), the Kay Kendall Leukaemia Fund, a Wellcome Trust strategic award to the Cambridge Institute for Medical Research (100140), a core support grant from the Wellcome Trust and MRC to the Wellcome Trust-Medical Research Council Cambridge Stem Cell Institute, the Connor Wright Project, the Cambridge National Institute for Health Research Biomedical Research Centre and the European Cooperation in Science and Technology (COST) Action CA18233 "European Network for Innovative Diagnosis and treatment of Chronic Neutropenias, EuNet INNOCHRON". YC is supported by the Scientific and Technical Foundation of Shanxi Province (grant no. 2020JM-015). We thank Dr. Irene E. Zohn for kindly providing the HectD1 WT and C2579G constructs. We are grateful to Drs. John Woolford and Sebastian Klinge for valuable advice and helpful discussions of this work.

Author contributions

W. T. conceived the project and supervised the studies. W. T., K. L. designed the experiments and wrote the manuscript with input from all authors. K. L. performed all the animal experiments with assistance of C. G. and H. X., who did animal dissection and flow cytometry. R.D. performed initial biochemistry and colony assays. Y. C. helped perform transplantation assay. K. L., C. G. and J. R. contributed to immunoblotting experiments. K. L., V. R. P, C. A. and C. G. designed and

performed polysome profiling assay. S.P. and A. J. W. contributed to ribosome assays and manuscript editing.

Declaration of interests

The authors declare no competing financial interests.

Inclusion and diversity

We worked to ensure sex balance in the selection of non-human subjects. The author list of this paper includes contributors from the location where the research was conducted who participated in the data collection, design, analysis, and/or interpretation of the work.

Main figure titles and legends

Figure 1. *Hectd1*-deficient BMs display a defective reconstituting ability and reduced functional HSC frequency.

- (A) Experimental scheme of serial BM transplantation assay.
- (B) Representative flow plots of donor/competitor/host chimerism in the peripheral blood (PB) of recipient mice after transplantation.
- (C) Donor chimerisms in the PB of recipient mice were measured every 4 weeks and the results are graphed. *Hectd1^{ff}* (n=11) and *Hectd1^{ff};Vav* (n=11).
- (D) Lineage reconstitutions of donor-derived cells in primary recipients at 16 weeks post-transplantation are shown. *Hectd1^{ff}* (n=11) and *Hectd1^{ff};Vav* (n=11).
- (E) Percentages of donor-derived HSPC subpopulation in the BM of primary transplanted mice at 16 weeks are shown. *Hectd1^{ff}* (n=6) and *Hectd1^{ff};Vav* (n=6).
- (F) Donor percentages in the PB of secondary BMT recipients were analyzed every four weeks and the results are graphed. *Hectd1^{ff}* (n=10) and *Hectd1^{ff};Vav* (n=11).
- (G) Experimental scheme of limiting dilution BMT to assess functional HSC frequency of *Hectd1^{ff}* and *Hectd1^{ff};Vav* BMs. (H) The results are presented as number of positively engrafted mice versus total number of mice analyzed for the indicated doses. Positive engraftment was defined as >1% donor-derived cells in the PB. CRU: competitive repopulating unit. 1SE: one standard deviation.
- (I) Donor chimerisms in the PB of recipient mice transplanted with different doses of BM cells at 16 weeks are shown. 100k: *Hectd1^{ff}* (n=5) and *Hectd1^{ff};Vav* (n=6); 30k: *Hectd1^{ff}* (n=10) and *Hectd1^{ff};Vav* (n=13); 10k: *Hectd1^{ff}* (n=9) and *Hectd1^{ff};Vav* (n=7). In all relevant panels, each symbol represents an individual mouse; bars indicate mean frequencies; error bars indicate SE. *: p<0.05; **: p<0.01; ***: p<0.001; ns: not significant, as determined unpaired by two-tailed Student's *t*-test.
- See also Figure S1, S2 and S3A-S3K.

Figure2. *Hectd1* is required for HSC self-renewal *in vivo* and maintenance *ex vivo*.

- (A) Experimental scheme of HSC transplantation assay. LT-HSCs (LSK CD150⁺CD48⁻) from *Hectd1^{ff}* and *Hectd1^{ff};Vav* mice were purified by flow cytometric sorting and 100 HSCs were either injected with 500K Sca1-depleted competitor BMs into lethally irradiated recipient mice (Day0-BMT) or the resultant culture after 12 days was injected with 300K BMs into recipient mice (Day12-BMT).
- (B) Donor chimerisms in the PB of recipient mice transplanted with fresh HSCs (day0-BMT) were measured every 4 weeks and the results are shown in the graph. *Hectd1^{ff}* (n=8) and *Hectd1^{ff};Vav* (n=8).
- (C) Percentages of donor-derived HSPC subpopulations in the BM of day0-BMT recipient mice 16 weeks post-transplant are shown. *Hectd1^{ff}* (n=6) and *Hectd1^{ff};Vav* (n=5).
- (D) Donor chimerisms of day12 cultured HSC transplants (Day12-BMT) in the PB of recipient mice were measured every 4 weeks and the results are shown in the graph. *Hectd1^{ff}* (n=7) and *Hectd1^{ff};Vav* (n=5).
- (E) Percentages of donor-derived HSPC subpopulations in the BM of day12-BMT recipient mice 16 weeks post-transplant are shown. *Hectd1^{ff}* (n=6) and *Hectd1^{ff};Vav* (n=4).
- (F) Representative images of *ex vivo* cultured HSCs at day 8.
- (G-I) Cell numbers of *ex vivo* cultured HSCs at different time points in different combinations of cytokines are shown. n=3 in each group.
- (J) Experimental scheme of HSC versus MPP/HPC transplantation assay. HSCs (LSK CD150⁺CD48⁻) or MPP/HPCs (LSK CD150⁻CD48⁺) were sorted from *Hectd1^{ff}* and *Hectd1^{ff};Vav* mice. 500 HSCs or 5000 MPP/HPCs were transplanted into each sub-lethally irradiated recipient

mice.

(K-L) Donor chimerisms in the PB of recipient mice were measured by flow cytometry every week post-BMT. Donor chimerisms of HSC (K) and MPP/HPC (L) transplants are shown. *Hectd1^{ff}* (n=7-9) and *Hectd1^{ff;Vav}* (n=6-7).

Data in (G-I) are represented by mean± SD. In all relevant panels, each symbol represents an individual mouse; bars indicate mean frequencies; error bars indicate SE. *: p<0.05; **: p<0.01; ***: p<0.001, as determined by unpaired two-tailed Student's *t*-test.

See also Figure S3L-S3M.

Figure 3. HectD1 interacts with, ubiquitinates, and degrades ZNF622.

(A) Freshly purified LSKs from *Hectd1^{ff}* and *Hectd1^{ff;Vav}* mice were used to examine various signaling molecules by WB using the indicated antibodies.

(B) TF-1/hMPL cells stably depleted of *HECTD1* using two different shRNAs were generated along with shRNA to Luciferase (Luc). Cell lysates were subjected to WB analysis using indicated antibodies.

(C, D) TF-1/hMPL shLuc or sh*HECTD1* cells were cultured in triplicates in different concentrations of GM-CSF (C) or TPO (D). Cell growth after 3 days' culture were determined by MTT absorbance.

(E) Silver staining gel image of a representative large-scale protein purification result to evaluate the efficiency and specificity of affinity purification of HA-HectD1 interacting proteins. * indicates the HA-HectD1 bait. IgG-H: indicates the Immunoglobulin heavy chain.

(F) CRAPome analysis of Hectd1-interacting proteins from three independent IP-MS results revealed the SAINT probability over fold changes. ZNF622 was identified as an Hectd1 interactor and highlighted in red.

(G) co-IP/WB analysis confirmed the interaction between Flag-ZNF622 and endogenous HectD1 in Flag-ZNF622 reconstituted TF-1 cells.

(H) ZNF622 protein levels were increased in *Hectd1^{ff;Vav}* LSKs compared to that of *Hectd1^{ff}* LSKs.

(I) Quantification of ZNF622 protein levels from three independent experiments as in (H) is plotted.

(J) ZNF622 mRNA levels were not affected in *Hectd1*-deficient LSKs as shown by qRT-PCR analysis. n=3 in each group.

(K) TF-1 cells stably depleted of *HECTD1* using two different shRNAs were treated with cycloheximide (CHX) for indicated times. ZNF622 half-lives were determined by WB. Representative blots of 3 independent experiments are shown. S.E., short exposure; L.E., long exposure.

(L) Relative ZNF622 levels normalized to Luc time 0 (left panel) and that normalized to respective time 0 (right panel) as shown in (J).

(M) 293T cells were transfected with HA-HectD1 or E3-dead mutant HectD1, along with Flag-ZNF622 and His-Ub or Ub mutant constructs as indicated. Cells were subjected to lysis in denatured condition followed by Ni²⁺ beads-pulldown. Ubiquitinated proteins were detected by WB using indicated antibodies.

In all relevant panels, data are represented by mean± SD. p-values are determined by unpaired two-tailed Students' *t*-test. *: p<0.05; **: p<0.01; ***: p<0.001

See also Figure S4.

Figure 4. *Hectd1* deficiency reduces HSC frequency and protein translational rate upon proliferative stress

(A-D) *Hectd1^{ff}* and *Hectd1^{ff;Vav}* mice were injected with 150mg/kg 5-FU, and euthanized at 10 days later for subsequent analysis.

(A) HSC and MPP numbers in the BM of 5-FU challenged *Hectd1^{ff}* (n=8) and *Hectd1^{ff;Vav}* (n=8) mice are shown.

(B) Representative histogram plot of protein synthesis rate in BM HSCs of 5-FU challenged mice as determined by *in vivo* OP-Puro assay.

(C) Quantification of protein synthesis rate in HSCs and MPPs of 5-FU challenged *Hectd1^{ff}* (n=6) and *Hectd1^{ff;Vav}* (n=5) mice as shown in (B).

(D) Percentages of BM HSCs and MPPs in the S phase of the cell cycle as determined by *in vivo* BrdU assay. *Hectd1^{ff}* (n=3) and *Hectd1^{ff;Vav}* (n=3).

(E-H) *Hectd1^{ff}* and *Hectd1^{ff;Vav}* mice were injected with cyclophosphamide (Cy) followed by two consecutive daily injections of G-CSF. Mice were euthanized one day after the last injection for subsequent analysis.

(E) HSC and MPP numbers in the BM of Cy+2GCSF challenged *Hectd1^{ff}* (n=7) and *Hectd1^{ff;Vav}* (n=7) mice. Data are pooled from 4 independent experiments and unique symbols indicate mice from different experiments.

(F) Representative histogram plot of protein synthesis rate in BM HSCs of *Hectd1^{ff}* and *Hectd1^{ff;Vav}* mice as determined by *in vivo* OP-Puro assay.

(G) Quantification of protein synthesis rate in HSCs and MPPs of *Hectd1^{ff}* (n=4) and *Hectd1^{ff;Vav}* (n=4) mice as shown in (F).

(H) Percentages of BM HSCs and MPPs in the S phase of the cell cycle as determined by *in vivo* BrdU assay. *Hectd1^{ff}* (n=3) and *Hectd1^{ff;Vav}* (n=4).

(I) Protein synthesis rates of 2-day cultured LSKs from *Hectd1^{ff}* and *Hectd1^{ff;Vav}* mice were determined by OP-puro incorporation of newly synthesized protein after 1hr labelling. Representative histogram plot is shown.

(J) Quantification of relative protein synthesis rates of 2-day cultured LSKs from three independent experiments using OP-Puro assays as shown in (I).

(K) Relative CFU-GM progenitors from *Hectd1^{ff}* (n=3) and *Hectd1^{ff;Vav}* (n=3) BMs in the presence of various concentrations of the translation elongation inhibitor puromycin is shown.

Data in (A, C, D, E, G and H) are represented by mean± SE. Data in (J, and K) are represented by mean± SD. p-value in (E) is determined by paired two-tailed Students' t-test; p-values in other panels are determined by unpaired two-tailed Students' t-test. *: p<0.05; **: p<0.01; ***: p<0.001; ns, not significant.

See also Figure S5.

Figure 5. *Hectd1* deficiency results in an accumulation of ZNF622 and eIF6 in the 60S and a reduction in ribosomal subunit joining, which is restored by ZNF622 depletion.

(A) Polysome profiling analysis of 2 day-cultured LSKs from *Hectd1^{ff}* and *Hectd1^{ff;Vav}* mice.

(B) Quantifications of 60S:40S ratio (left panel) and 60S:80S ratio (right panel) from polysome profiling assay of TF-1 cells expressing shLuc or sh*HECTD1*. Three independent experiments were performed.

(C) Fractions from sucrose gradients (7%-45%) of TF-1 cell lysates stably expressing shLuc or sh*HECTD1* were collected and subjected to WB analysis. Representative result of three independent experiments is shown. Fractions 1-3 are cytoplasmic soluble proteins. 40S, 60S, 80S monosome and polysome fractions are indicated by colored lines, arrows, and fonts. Whole cell lysate (WCL). AF: assembly factor; RPL: ribosome protein large unit; RPS: ribosome protein small unit. WCL and sucrose fractions (shLuc and sh*HECTD1*) were resolved in three SDS-PAGE gels in parallel. Sucrose fraction immunoblots were processed and developed in parallel, and images presented side-by-side.

(D) Quantification of relative protein distribution in different polysome fractions as shown in (C). Relative protein levels in each fraction was normalized to the peak fraction of the indicated protein from the shLuc cells and plotted. n=3-4.

(E-J) Knockdown of *ZNF622* in *HECTD1*-deficient cells rescues ribosome composition, eIF6 release, as well as 60S/40S joining.

(E) WB examination of knockdown efficiency in shLuc, *HECTD1* single and *HECTD1*;*ZNF622* double knockdown (DKD) cells.

(F) Representative polysome profiles of TF-1 shLuc, *HECTD1* and DKD cells.

(G) Quantifications of 60S:40S ratio (left panel) and 60S:80S ratio (right panel) of polysome profiles as shown in (F). n=3.

(H) Representative result of WB analysis with protein fractions from sucrose gradients (7%-45%) of TF-1 shLuc, *HECTD1* and DKD cells (top panel). Quantification of eIF6 distribution in polysome fractions (bottom panel). N=3.

(I) Ribosome dissociation/reassociation assay. Indicated TF-1 cell lines were lysed in 0.25mM low Mg^{2+} buffer to dissociate ribosomal subunits (Top graph). $MgCl_2$ was subsequently added to a final concentration of 10mM for ribosomal subunit reassociation (Bottom graph). Resultant cell lysates were loaded on a 7-45% sucrose gradient profiled. Representative graphs from three independent experiments are shown.

(J) Quantification of 60S:40S ratios in the dissociated profiles (Top panel) and 80S:40S ratios in the reassociated profiles (Bottom panel). N=3. Note that the black line (shLuc) and the blue line (DKD) in (F, H and I) superimpose.

All data are represented by mean \pm SD. p-values are determined by unpaired two-tailed Students' t-test. *: p<0.05; **: p<0.01; ***: p<0.001; ns, not significant.

See also Figure S6A-S6F.

Figure 6. Knockdown of *Znf622* in *Hectd1*-deficient cells restores protein synthesis rate and HSC reconstitution ability.

(A) TF-1 cells stably expressing control shLuc, single or double knockdown of *HECTD1* and *ZNF622* were generated by lentiviral infection and sorting. WB analysis with indicated antibodies is shown.

(B) Global protein synthesis rates of various TF-1 cells as in (A) were measured using OP-Puro assay.

(C) Knockdown efficiency of 3 different shRNAs to mouse *Znf622* in BaF3 cells is shown. shRNA #1 and #2 are chosen for subsequent BMT.

(D) Schematic illustration of HSC lentiviral transduction/BMT strategy.

(E) mCherry⁺ donor fractions in the PB were analyzed every 4 weeks post-BMT. Quantifications of mCherry⁺% within donor from each group are shown. *flf*;*Vav*+shLuc, n=5; *flf*;*Vav*+sh*Znf622*#1, n=6; *flf*;*Vav*+sh*Znf622*#2, n=5.

(F) Quantifications of mCherry⁺ donor% in the HSC and MPP fractions 16-weeks post BMT are shown. *flf*;*Vav*+shLuc, n=5; *flf*;*Vav*+sh*Znf622*#1, n=3; *flf*;*Vav*+sh*Znf622*#2, n=4.

(G) In a separate experiment, LSK cells were purified from *Hectd1*^{flf} and *Hectd1*^{flf};*Vav* mice, infected with lentivirus expressing shLuc or sh*Znf622*#1, and subsequently transplanted. Quantifications of mCherry⁺ donor% in the PB from each group are shown. *flf* +shLuc, n=8; *flf*+sh*Znf622*#1, n=8; *flf*;*Vav*+shLuc, n=7; *flf*;*Vav*+sh*Znf622*#1, n=7.

(H) Quantifications of mCherry⁺ donor percentages in the HSC and MPP fractions at the end of primary BMT are shown. *flf* +shLuc, n=8; *flf*+sh*Znf622*#1, n=8; *flf*;*Vav*+shLuc, n=7; *flf*;*Vav*+sh*Znf622*#1, n=7.

(I) Two million BM cells from primary transplanted mice were harvested and transplanted into each secondary recipient. Quantifications of mCherry⁺ % within donor from each group in the

secondary transplants are shown. *f/f +shLuc*, n=16; *f/f+shZnf622#1*, n=13; *f/f;Vav+shLuc*, n=14; *f/f;Vav+shZnf622#1*, n=9.

In all relevant experiments, each symbol represents an individual mouse; horizontal lines indicate mean frequencies; error bars indicate SE. *: p<0.05; **: p<0.01; ***: p<0.001; ns, not significant, as determined by unpaired two-tailed Student's *t*-test.

See also Figure S6G.

Supplemental Excel Table titles and legends

Table S1. Fold enrichment changes and SAINT score for HectD1 interacting proteins by IP/MS. Related to Figure 3.

Table S2. Genotyping and qPCR primers used. Related to STAR Methods.

STAR★METHODS

KEY RESOURCES TABLE

REAGENT or RESOURCE	SOURCE	IDENTIFIER
Antibodies		
Rabbit polyclonal anti-HectD1	Bethyl lab	Cat# A302-908A, RRID:AB_10664800
Rabbit polyclonal anti-ZNF622	Bethyl lab	Cat# A304-075A, RRID:AB_2621324
Rabbit polyclonal anti-NOB1	Bethyl lab	Cat# A304-680A, RRID:AB_2620875
Rabbit polyclonal anti-RPS3	Bethyl lab	Cat# A303-840A, RRID:AB_2620191
Rabbit polyclonal anti-RPL23A	Proteintech	Cat# 16386-1-AP, RRID:AB_2269755
Rabbit polyclonal anti-RPL24	Proteintech	Cat# 17082-1-AP, RRID:AB_2181728
Rabbit polyclonal anti-eIF6	Proteintech	Cat# 10291-1-AP, RRID:AB_2096515
Rabbit polyclonal anti-NMD3	Proteintech	Cat# 16060-1-AP, RRID:AB_2282830
Rabbit polyclonal anti-DNAJC21	Proteintech	Cat# 23411-1-AP, RRID:AB_2879274
Mouse monoclonal anti-PA2G4	Proteintech	Cat# 66055-1-Ig, RRID:AB_11042597
Rabbit polyclonal anti-RPL11	Abcam	Cat# ab79352, RRID:AB_2042832
Rabbit monoclonal anti-RPL11	Abcam	Cat# ab32157, RRID:AB_732117
Mouse monoclonal anti- GSK3 α / β	Millipore	Cat# 368662-200UG, RRID:AB_2043310
Mouse monoclonal anti-HSP90	StressMarq	Cat# SMC-107, RRID:AB_854214
Mouse monoclonal anti- β -Catenin	BD Biosciences	Cat# 610153, RRID:AB_397554
Goat monoclonal anti-Actin	Santa Cruz	Cat# sc-1616, RRID:AB_630836
Rabbit polyclonal anti-STAT5	Santa Cruz	Cat# sc-835, RRID:AB_632446
Rabbit monoclonal anti-pY1007/1008-JAK2	Cell Signaling	Cat# 3776, RRID:AB_2617123
Rabbit monoclonal anti-JAK2	Cell Signaling	Cat# 3230, RRID:AB_2128522
Rabbit polyclonal pY694-STAT5	Cell Signaling	Cat# 9351, RRID:AB_2315225
Rabbit polyclonal anti-pS473-AKT	Cell Signaling	Cat# 9271, RRID:AB_32982
Rabbit polyclonal anti-AKT	Cell Signaling	Cat# 9272, RRID:AB_329827
Mouse monoclonal anti-pT202/204-ERK1/2	Cell Signaling	Cat# 9106, RRID:AB_331768
Rabbit polyclonal anti-ERK1/2	Cell Signaling	Cat# 9102, RRID:AB_330744
Rabbit monoclonal anti-pS2448-mTOR	Cell Signaling	Cat# 5536, RRID:AB_10691552
Mouse monoclonal anti-mTOR	Cell Signaling	Cat# 4517, RRID:AB_1904056
Mouse monoclonal pT389-S6K1	Cell Signaling	Cat# 9206, RRID:AB_2285392
Rabbit polyclonal anti-S6K1	Cell Signaling	Cat# 9202, RRID:AB_331676
Rabbit monoclonal anti-pS235/236-RPS6	Cell Signaling	Cat# 4858, RRID:AB_916156
Rabbit polyclonal anti-pS240/244-RPS6	Cell Signaling	Cat# 2215, RRID:AB_331682
Rabbit monoclonal anti-RPS6	Cell Signaling	Cat# 2217, RRID:AB_331355
Rabbit monoclonal anti-pT37/46-4E-BP1	Cell Signaling	Cat# 2855, RRID:AB_560835
Rabbit monoclonal anti-4E-BP1	Cell Signaling	Cat# 9644, RRID:AB_2097841
Rabbit polyclonal anti-pS21/9-GSK3 α / β	Cell Signaling	Cat# 9331, RRID:AB_329830
Rabbit polyclonal anti-eIF2 α	Cell Signaling	Cat# 9722, RRID:AB_2230924
Rabbit monoclonal anti- β -Tubulin	Cell Signaling	Cat# 2128, RRID:AB_823664
Mouse monoclonal anti-GAPDH	Cell Signaling	Cat# 97166, RRID:AB_2756824
Rabbit monoclonal anti-HA	Cell Signaling	Cat# 3724, RRID:AB_1549585
Mouse monoclonal anti-FLAG M2-HRP	Sigma-Aldrich	Cat# A8592, RRID:AB_439702
Digital anti-mouse HRP	Kindle Biosciences	Cat# R1005, RRID:AB_2800463
Digital anti-Rabbit HRP	Kindle Biosciences	Cat# R1006, RRID:AB_2800464
CD45.1-FITC	BD Biosciences	Cat# 553775, RRID:AB_395043
CD45.1-PE-Cy7	Thermo Fisher	Cat# 25-0453-82, RRID:AB_469629
CD45.1-eF450	Thermo Fisher	Cat# 48-0453-82, RRID:AB_1272189
CD45.2-APC-Cy7	Thermo Fisher	Cat# 47-0454-82, RRID:AB_1272175
CD45.2-Buv395	BD Biosciences	Cat# 564616, RRID:AB_2738867
Gr1-PE	Thermo Fisher	Cat# 12-5931-83, RRID:AB_466046
Mac1-APC	Thermo Fisher	Cat# 17-0112-83, RRID:AB_469344
B220-PE	BD Biosciences	Cat# 553090, RRID:AB_394620
B220-APC	Thermo Fisher	Cat# 17-0452-83, RRID:AB_469396

CD4-PE	BD Biosciences	Cat# 553049, RRID:AB_394585
CD8a-PE	BioLegend	Cat# 100707, RRID:AB_312746
CD3e-FITC	Thermo Fisher	Cat# 11-0031-82, RRID:AB_464882
CD3e-PE	Thermo Fisher	Cat# 12-0031-85, RRID:AB_465498
Ter119-biotin labeled	Thermo Fisher	Cat# 13-5921-85, RRID:AB_466798
Gr1-biotin labeled	Thermo Fisher	Cat# 13-5931-86, RRID:AB_466802
Mac1-biotin labeled	Thermo Fisher	13-0112-86, RRID:AB_466361
B220-biotin labeled	Thermo Fisher	Cat# 13-0452-86, RRID:AB_466451
CD19-biotin labeled	Thermo Fisher	Cat# 13-0193-86, RRID:AB_657655
CD4-biotin labeled	Thermo Fisher	Cat# 13-0041-86, RRID:AB_466327
CD5-biotin labeled	Thermo Fisher	Cat# 13-0051-85, RRID:AB_466340
CD8a-biotin labeled	Thermo Fisher	Cat# 13-0081-86, RRID:AB_466348
Streptavidin-PE-TexasRed	Thermo Fisher	Cat# SA1017, RRID:N/A
Streptavidin-APC-Cy7	Thermo Fisher	Cat# 47-4317-82, RRID:AB_10366688
c-Kit-PE	BD Biosciences	Cat# 553355, RRID:AB_394806
c-Kit-APC	Thermo Fisher	Cat# 17-1171-83, RRID:AB_469431
c-Kit-APC-Cy7	Thermo Fisher	Cat# 47-1171-82, RRID:AB_1272177
Sca1-PE	BD Biosciences	Cat# 553336, RRID:AB_394792
Sca1-PerCp-Cy5.5	Thermo Fisher	Cat# 45-5981-82, RRID:AB_914372
CD150-PE-Cy7	BioLegend	Cat# 115914, RRID:AB_439797
CD48-FITC	BioLegend	Cat# 103403, RRID:AB_313018
CD48-APC-Cy7	BioLegend	Cat# 103432, RRID:AB_2561463
CD48-AF700	BioLegend	Cat# 103426, RRID:AB_10612755
CD48-APC	Thermo Fisher	Cat# 17-0481-82, RRID:AB_469408
Flk2-PE	BD Biosciences	Cat# 553842, RRID:AB_395079
CD34-APC	Thermo Fisher	Cat# 50-0341-82, RRID:AB_10596826
CD16/32-PE	BD Biosciences	Cat# 553145, RRID:AB_394660
Bacterial and Virus Strains		
pCL20.MSCV.mir30.PGK.mCherry	Holmfeldt et al., 2016	N/A
pCL20.MSCV.mir30.PGK.GFP	This paper (Replace mCherry with GFP)	N/A
Chemicals, Peptides, and Recombinant Proteins		
5-Fluorouracil (5-FU)	Sigma-Aldrich	Cat# F6627
Cyclophosphamide	Baxter	Cat# NDC 10019-955-01
O-Propargyl-Puromycin (OP-Puro)	MedChemExpress	Cat# HY-15680/CS-6850
BrdU	BD Pharmingen	Cat# 5133284
Puromycin dihydrochloride	Sigma-Aldrich	Cat# P7255
Insulin Solution Human	Sigma-Aldrich	Cat# I9278
10% BSA in IMDM	StemCell Technologies	Cat# 09300
L-Glutamine	Gibco	Cat# 25030-081
Holo-Transferrin human	Sigma-Aldrich	Cat# T0665
β -Mercaptoethanol	Sigma-Aldrich	Cat# M3148
Propidium iodide (PI)	Sigma-Aldrich	Cat# P4170
DAPI	Sigma-Aldrich	Cat# D9542
3% Acetic Acid with Methylene Blue	StemCell Technologies	Cat# 07060
Retronectin	Takara	Cat# T100B
Cycloheximide	Sigma-Aldrich	Cat# C7698
Imidazole	Acros Organics	Cat# 288-32-4
N-Ethylmaleimide (NEM)	Sigma-Aldrich	Cat# E1271
PR619	LifeSensors	Cat# SI9619
1,10-phenanthroline	Mallinckrodt Chemicals	Cat# 2631-55
Sodium Fluoride	Sigma-Aldrich	Cat# S7920
Sodium orthovanadate	Sigma-Aldrich	Cat# 450243
PMSF	Sigma-Aldrich	Cat# P7626
Protease Inhibitor Cocktail Tablets; EDTA-free	Roche	Cat# 11836170001
Protease Inhibitor Cocktail Tablets	Roche	Cat# 11697498001
Bovine Serum Albumin (BSA)	Fisher Bioreagents	Cat# BP1600

Nonfat milk	Santa Cruz	Cat# sc2325
StemSpan SFEM	StemCell Technologies	Cat# 09600
Fetal Bovine Serum	SAFC Biosciences	Cat# 12103C
Bovine Calf Serum	HyClone	Cat# SH30072.03
HA peptide	Thermo Fisher	Cat# 26184
Anti-HA Affinity Gel	Sigma-Aldrich	Cat# E6779
Anti-FLAG M2 Affinity Gel	Sigma-Aldrich	Cat# F2426
Protein A Sepharose CL-4B	GE Health	Cat# 17-0780-01
Protein G Sepharose 4 Fast Flow	GE Health	Cat# 17-0618-01
HisPur Ni-NTA Resin	Thermo Fisher	Cat# 88221
Murine SCF	Peptotech	Cat# 250-03
Murine Tpo	Peptotech	Cat# 315-14
Murine IL3	Peptotech	Cat# 213-13
Murine FLT3L	Peptotech	Cat# 250-31L
Murine IL6	Peptotech	Cat# 216-16
rh EPO	Espogen	Cat# NDC 55513-144-10
rG-CSF (Neupogen)	Amgen	Cat# NDC 55513-209-01
Human GM-CSF	Peptotech	Cat# 300-03
Human TPO	Peptotech	Cat# 300-18
Critical Commercial Assays		
Lineage Cell Depletion Kit mouse	Miltenyi Biotec	Cat# 130-090-858
Anti-Sca-1 Microbead Kit (FITC)	Miltenyi Biotec	Cat# 130-092-529
Click-iT Plus OP-Puro Protein Synthesis Kit	Thermo Fisher	Cat# C10458
FITC Annexin V Apoptosis Detection Kit	BD Pharmingen	Cat# 556547
BrdU Flow Kits	BD Pharmingen	Cat# 557891
BD Cytotfix/Cytoperm	BD Biosciences	Cat# 554714
SYBR Green Master Mix	Applied Biosystems	Cat# 43-091-55
RNeasy Plus Mini Kit	QIAGEN	Cat# 74136
qScript cDNA Supermix	Quanta Biosciences	Cat# 98047
Experimental Models: Cell Lines		
TF-1	ATCC	Cat# CRL-2003, RRID:CVCL_0559
HEK293T	ATCC	Cat# CRL-3216, RRID:CVCL_0063
WEHI-3B	Dr. Harvey Lodish lab	RRID:CVCL_2239
BaF3	DSMZ	Cat# ACC-300, RRID:CVCL_0161
Experimental Models: Mouse Strains		
C57B6/NGpt- <i>Hectd1</i> ^{tm1b} /Gpt	EuComm and MARC, China	Cat# 5757216, RRID:MGI:5757216
<i>FLP</i> B6;SJL-Tg(ACTFLPe)9205Dym/J	Jackson laboratories	Cat# JAX:003800, RRID:IMSR_JAX:003800
<i>Vav-Cre</i> mice	Stadtfeld and Graf, 2005; Chen et al., 2009	N/A
C57BL/6J (CD45.2)	Jackson laboratories	Cat# 000664
SJL (CD45.1)	Jackson laboratories	Cat# 000686
Oligonucleotides		
sh human <i>HECTD1</i> #1: tatgaacaagattgtagtcaa	This paper	N/A
sh human <i>HECTD1</i> #2: taccactggtgttcaactcta	This paper	N/A
sh human <i>ZNF622</i> #1: atcggaaagtggagatgatgaa	This paper	N/A
sh human <i>ZNF622</i> #2: tggagacgattgggaagatatt	This paper	N/A
sh mouse <i>Znf622</i> #1: agagaaagttggtgttgcaaa	This paper	N/A
sh mouse <i>Znf622</i> #2: tgtgacagttgctaggaatcaa	This paper	N/A
Oligonucleotides for mouse genotyping and real-time qPCR see Table S2	This paper	N/A
Recombinant DNA		
pCMV-HA-HectD1 WT	Sarkar and Zohn, 2012	N/A
pCMV-HA-HectD1 C2579G	Sarkar and Zohn, 2012	N/A
pCMV-HA-HectD1 truncates/deletion mutants	This paper	N/A
pOZ-FH-ZNF622 full length	This paper	N/A

pOZ-FH-ZNF622 truncates/deletion mutants	This paper	N/A
pOZ-Flag-ZNF622	This paper	N/A
Softwares and Algorithms		
Flowjo	https://www.flowjo.com/solutions/flowjo	RRID:SCR_008520
GraphPad Prism	http://www.graphpad.com/	RRID:SCR_002798
Fiji	http://fiji.sc	RRID:SCR_002285
QuantStudio Real-Time PCR software	Thermo Fisher	https://www.thermofisher.com/us/en/home/life-science/pcr/real-time-pcr/
SAINT	Choi et al., 2012	http://saint-apms.sourceforge.net/Main.html
ELDA	Hu and Smyth, 2009	http://bioinf.wehi.edu.au/software/elda/
Sequest	Eng et al., 1994	http://tools.thermofisher.com/content/sfs/manuals/Man-XCALI-97160-SEQUEST-331-User-ManXCALI97160-B-EN.pdf

RESOURCE AVAILABILITY

Lead Contact

Further information and requests for resources and reagents should be directed to and will be fulfilled by the Lead Contact, Wei Tong (tongw@chop.edu).

Materials Availability

This study did not generate new unique reagents.

Data and Code Availability

This study did not generate new datasets.

EXPERIMENTAL MODEL AND SUBJECT DETAILS

Mouse models

Hectd1 “knockout-first, conditional-ready” mouse line (C57B6/NGpt-*Hectd1*^{tm1a}/Gpt, #T000502) was obtained from EuComm (the ES lines were generated by European Consortium) and Model Animal Resource Information Platform of Nanjing University, China. *FLP1* recombinase transgenic mice (B6;SJL-Tg(ACTFLPe)9205Dym/J, #003800) and SJL (CD45.1) recipient mice were purchased from the Jackson Laboratory (Rodriguez et al., 2000). *Vav1-Cre* mice were originally generated by Dr. Thomas Graf (Stadtfeld and Graf, 2005) and generously provided by Dr. Nancy Speck (Chen et al., 2009). *Hectd1* transgenic mice were first crossed with *Rosa-Flippase* mice to eliminate FRT-flanked LacZ and Neo mini-gene, and then with wild type mice to get rid of the *Rosa-Flippase* gene to minimize the possible effects of these elements in hematopoiesis. The resultant mice with loxP-flanked *Hectd1* alleles (*Hectd1*^{ff}) targeting exon 3 were crossed with *Vav-cre* transgenic mice to obtain the control *Hectd1*^{ff} and *Hectd1*^{ff;Vav} conditional knockout mice (cKO). All mice were bred and grown in house in pathogen-free animal facilities. Both male and female mice (8~12 weeks old) were used and randomly assigned for all experiments. All the animal studies were performed under an approved protocol by the Institutional Animal Care and Use committee of the Children’s Hospital of Philadelphia.

For 5-FU challenge, sex and age-matched (8~12 weeks old) adult *Hectd1*^{ff} and *Hectd1*^{ff;Vav} mice were injected intraperitoneally with 5-Fluorouracil (5-FU, Cat#F6627, Sigma, 150mg/kg body

weight, pH8.5 in PBS) (Rozenova et al., 2015). Total BM cell count, HSC frequency, cell cycle and apoptosis assay were determined after 10 days of 5-FU administration. For Cy/GCSF induced stress, we intraperitoneally injected mice with 1 dose of cyclophosphamide (4mg/mouse, Baxer) followed by two daily subcutaneous injections of 5ug GCSF (Neupogen, Amgen). 1 day after the last GCSF injection, mice were euthanized for subsequent analysis (Morrison et al., 1997; Signer et al., 2014).

Cell lines

TF-1 cell lines were purchased from American Type Culture Collection (ATCC) and grown in RPMI-1640 media supplemented with 10% bovine calf serum (Cat# SH30072.03, HyClone), 2mM L-glutamine (Cat# 25030-081, Gibco) and penicillin/Streptomycin (Gibco) and 2ng/mL GM-CSF (PeproTech) at 37°C and 95% humidity in an atmosphere of 5% CO₂. 293T cells were from ATCC and grown in DMEM media supplemented with 10% bovine calf serum, 2mM L-glutamine and penicillin/Streptomycin at 37°C and 95% humidity in an atmosphere of 5% CO₂. BaF3 cells were maintained in RPMI-1640 media supplemented with 10% bovine calf serum and 10% WEHI supernatant at 37°C and 95% humidity in an atmosphere of 5% CO₂.

METHOD DETAILS

Genotyping and qPCR

Mouse tail genomic DNAs were isolated with the standard proteinase K lysis protocol. Genotyping was performed by PCR. To evaluate *Vav-cre* excision efficiency in hematopoietic stem and progenitor cells, we plated total BM cells into M3434 methylcellulose semisolid media (StemCell Technologies Inc) for colony formation. Single colonies were picked, resuspended in 90uL buffer (50mM NaOH, 0.2mM EDTA), and boiled for 20min, followed by mixing with 10uL 1M Tris, pH8.0 for neutralization. The lysates were subsequently used for genotyping. Sequences of genotyping primers are listed in Table S2.

For quantitative real time PCR assay, total RNA was extracted using RNeasy Mini Kit (Qiagen). Reverse-transcription reaction was performed with random primers using qScript cDNA Supermix (Quanta Biosciences), and quantitative PCR was done with SYBR Green Master Mix (Applied Biosystems). Sequences of qPCR primers are listed in Table S2.

Constructs and virus packaging

pCMV-HA-HectD1 WT or C2579G mutant constructs were kindly gifted by Dr. Irene E. Zohn (Children's Research Institute, United States, Washington, DC, United States) (Sarkar and Zohn, 2012). The truncation mutants were amplified by PCR and subcloned into pCMV-HA vector. Human *ZNF622* cDNA was amplified by PCR from a homemade cDNA library from TF-1 cells and constructed into a retroviral pOZ-FH vector that contains a Flag and a HA tag. All the deletion or truncation mutants were subcloned into the pOZ-FH vector. HectD1 or ZNF622 miR30-based shRNA constructs were subcloned into Lentiviral vector (pCL20.MSCV.mir30.PGK.mCherry) generously provided by Dr. Shannon McKinney-Freeman

Complete blood count (CBC), flow cytometry of HSPCs and lineage cells

Peripheral blood was collected from 8~12 week-old *Hectd1^{fl/fl}* and *Hectd1^{fl/fl;Vav}* mice into EDTA-coated tubes. CBC analysis was performed with a Hemavet 950 (Drew Scientific, Inc). For lineage staining, cells from peripheral blood were lysed with RBC lysis buffer (0.8% NH₄Cl, 10uM EDTA, pH 7.4~7.6) for 10min at 4°C to remove red blood cells, followed by staining with different fluorochrome-conjugated anti-Gr-1 (RB6-8C5) (granulocytes), -Mac1 (M1/70) (macrophages), -

B220 (RA3–6B2) (mature B cells), -CD4 (GK1.5) and -CD8 (53–6.7) (T cells) antibodies, for 30min at 4°C. After washing with flow buffer (PBS containing 0.5% BSA), cells were suspended in flow buffer containing 1µg/mL propidium iodide (PI) or 2.5µg/mL DAPI for flow cytometry analysis.

HSPCs staining was conducted as described previously (Lv et al., 2017). Cells from BM (2 femurs+2 tibias+2 hips for one mouse) or spleen were harvested in PBS containing 0.5% BSA, and quickly lysed with RBC lysis buffer for 1min at 4°C. Cells were then stained with biotin-conjugated anti-Gr-1 (RB6–8C5), -Mac1 (M1/70), -B220 (RA3–6B2), -CD19 (eBio1D3), -Ter119 (TER-119), -CD5 (53–7.3), -CD4 (GK1.5), -CD8 (53–6.7), in combination with APC-Cy7-c-Kit (2B8), PerCP-Cy5.5-Sca1 (E13–161.7 or D7), FITC-CD48 (HM48–1), PE-Cy7-CD150 (TC15–12F12.2), APC-CD34 (RAM34), and PE-Flk2 (A2F10.1) antibodies for 30min on ice, followed by secondary staining with streptavidin-PE-TexasRed (Invitrogen SA1017, 1:50) for 30min on ice. Different HSPC subpopulations were defined as long-term stem cells (LT-HSCs, Lin⁻Scal⁺c-Kit⁺Flk2⁻CD150⁺CD48⁻), short-term stem cells (ST-HSCs, Flk2⁻CD150⁻CD48⁻ LSK), multiple potent progenitors (megakaryocyte/erythroid-biased MPP2, Flk2⁻CD150⁺CD48⁺ LSK; myeloid-biased MPP3, Flk2⁻CD150⁻CD48⁺ LSK; lymphoid-biased MPP4, Flk2⁺CD150⁻LSK) (Pietras et al., 2015).

For committed progenitor cell staining, namely granulocyte-monocyte progenitor (GMP, CD34⁺CD16/32⁺ Lin⁻c-Kit⁺Scal⁻) cells, common myeloid progenitor (CMP, CD34⁺CD16/32⁻ LKS⁻) cells and megakaryocyte-erythrocyte progenitor (MEP, CD34⁺CD16/32⁻ LKS⁻), cells from the BM or spleen were stained with PE-FrR111/II (CD16/CD32) for 30min on ice after a quick RBC lysis, followed by blocking with rat serum, then stained with biotin-conjugated lineage panel as described above, along with APC-Cy7-c-Kit (2B8), PerCP-cy5.5-Sca1 (E13–161.7 or D7), APC-CD34 for 1h on ice.

Lineage cell FACS samples were analyzed on a BD FACS Canto flow cytometer, while HSPC and progenitor samples were analyzed on a BD FACS Fortessa flow cytometer. Data were analyzed on FlowJo (FlowJo, LLC).

Competitive BMT and limiting dilution BMT

For competitive BMT, 1 million total BM cells from 8~12-week-old *Hectd1^{ff}* or *Hectd1^{ff};Vav* (CD45.2) mice were mixed with the same number of competitor total BM cells (CD45.1), and transplanted into lethally irradiated (a split dose of 10Gy) recipient mice (CD45.1/2) by retro-orbital injection. Every four weeks after BMT, donor cell reconstitution in periphery blood (PB) was evaluated by flow cytometry. 16 weeks after BMT, reconstituted donor stem and progenitor cells (HSPCs) from BM or spleen were analyzed by flow cytometry.

For limiting dilution BMT, an increasing number (10k, 30k, 100k) of total BM cells from *Hectd1^{ff}* or *Hectd1^{ff};Vav* (CD45.2) mice were mixed with a fixed number (300k) of competitor BM cells and transplanted into lethally irradiated recipient mice (Bersenev et al., 2008). 16 weeks after BMT, donor cell percentage in the PB was evaluated by flow cytometry. Mice with more than 1% of donor-derived cells were defined as “positive”. Data were analyzed by ELDA (Hu and Smyth, 2009).

HSC sorting and transplantation

HSC purification and BMT were performed as described previously (Balcerek et al., 2018). Lineage positive cells were first depleted using a lineage cell depletion kit (Cat# 130-090-858, Miltenyi Biotec). Lineage negative (Lin⁻) cells were then stained with APC-Cy7-c-Kit (2B8),

PerCP-Cy5.5-Sca1 (E13–161.7 or D7), FITC-CD48 (HM48–1), PE-Cy7-CD150 (TC15–12F12.2). LT-HSCs were purified with MoFlo Astrios Sorter and 100 LT-HSCs were seeded in a round-bottom 96-well plate. These LT-HSCs were either transplanted on the day (D0 BMT) or cultured in SFEM media supplemented with 100 ng/mL SCF and 20 ng/mL TPO for 12 days, and all the resultant cells were then transplanted (Day12 BMT). Specifically, 100 LT-HSCs (D0 BMT) or 100 LT-HSCs-derived cells (CD45.2) at day12 (D12 BMT) were mixed with 500k Sca1-depleted competitor BM cells (CD45.1 or CD45.1/2) and injected retro-orbitally into lethally irradiated (10Gy) recipient mice (CD45.1/2 or CD45.1). Every four weeks after BMT, donor cell reconstitution in the PB was evaluated by flow cytometry. 16 weeks after BMT, reconstituted donor stem and progenitor cells (HSPCs) from BM or spleen were analyzed by flow cytometry.

OP-Puro (O-propargyl-puromycin) Click-iT protein synthesis assay

To detect protein synthesis rate *in vivo*, primary or stressed mice were injected intraperitoneally with OP-Puro (Cat# HY-15680, MCE; 50mg/kg body weight, pH6.4-6.6 in PBS) for 1 hour before euthanasia (Signer et al., 2014). Total BM cells were harvested and live stained with cell surface markers for HSCs/MPPs after a quick RBC lysis. Cells were then fixed with BD Cytotfix solution for 20min on ice. After washing with BD Perm/Wash buffer, cells were permeabilized with BD Cytoperm Plus solution for 10min on ice, followed by refixing in Cytotfix solution for 5min. The azide-alkyne reaction was performed using Click-iT plus OPP Alexa Fluor 647 or 488 kit (Cat# C10458, Invitrogen) for 30min at room temperature. Cells were then washed and resuspended in flow buffer, and analyzed by on a BD FACS Fortessa flow cytometer.

For *ex vivo* analysis, OP-Puro was added to cell culture at the final concentration of 20uM for 1 hour at a 37°C incubator. The azide-alkyne reaction was performed as described above.

Cell cycle and cell apoptosis assay

For BrdU cell cycle analysis, mice were injected with 200uL BrdU (10mg/mL, Cat# 550891, BD Pharmingen) for 2 hours. Total BM cells were stained with cell surface markers for HSCs/MPPs, and then fixed and permeabilized with BD Cytotfix/Cytoperm kit, followed by treatment with 300ug/mL DNaseI for 1 hours at a 37°C water bath. After washing with BD Perm/Wash buffer, cells were stained with FITC-anti-BrdU (Cat# 5133284, BD Pharmingen) for 20min at room temperature. After washing, cells were resuspended in flow buffer with DAPI (5ug/mL), and analyzed by flow cytometry.

For apoptosis assay, total BM cells were stained with cell surface markers for HSCs/MPPs. After washing with flow buffer, cells were resuspended in 200uL Annexin V binding buffer. 10uL FITC-Annexin V (Cat# 55647, BD Pharmingen) and DAPI were added for 15min at room temperature in the dark, followed by adding 800uL binding buffer. Samples were analyzed on a BD Fortessa cytometer within 1 hour.

Viral transduction of LSK cells and transplantation

For LSK lentiviral infection and rescue BMT, sorted LSK cells from either *Hectd1^{fl/fl}* or *Hectd1^{fl/fl};Vav* (CD45.2) mice were cultured in SFEM media (StemCell Technologies Inc) supplemented with 10% FBS (SAFC Biosciences) and cytokines (100 ng/mL mSCF, 20 ng/mL mTpo, 20 ng/mL FLT3L, 20 ng/mL IL6) for 2 days. Lentivirus carrying mCherry/shLuc or mCherry/shmZNF622 were preloaded twice into a RetroNectin (T100B, Takara)-coated 12-well plate (Modlich et al., 2009). Cultured LSKs were transferred to the lentivirus-preload plates and incubated for one more day. At day3, 250k cultured LSKs were mixed with 500k Sca1-depleted competitor BM cells and injected into lethally-irradiated recipient mice. A small fraction of infected cells was spared for flow cytometry to evaluate the viral infection efficiency (Jiang et al., 2012).

Immunoprecipitation (IP)

For each anti-HA immunoprecipitation, ten ~80% confluent 10cm dishes of 293T cells were transiently transfected with pCMV-HA empty vector (control) or pCMV-HA-HectD1. 48 hours after transfection, cells were lysed with IP buffer (10mM Tris, pH7.4, 150mM NaCl, 0.5% NP-40, 1mM NaF, 1mM Na₃VO₄, PMSF, protease inhibitor cocktail, 10 μM PR-619 (LifeSensors), 4mM 1,10-phenanthroline (o-PA; Mallinckrodt Chemicals), 4mM N ethylmaleimide (NEM; Sigma-Aldrich)) for 30 min at 4°C. Cell lysates were clarified by centrifugation at 13,000 rpm for 10 min at 4°C, and then pre-cleared with protein A/G beads for 30 min.

HA-EZ Agarose beads (E6779, Sigma) were prepared by being sequentially washed with 0.1M pH2.5 Glycine, twice in 1M pH8.0 Tris buffer, and twice in IP buffer. Precleared supernatants were incubated with 100uL washed HA-EZ Agarose beads for 4 hrs with gentle agitation. We transferred the IPs to BioRad Micro Bio-Spin Chromatography Columns (Cat# 732-6204), and washed columns with 1mL IP buffer for four times, followed by a quick spin down to drain the leftover IP buffer. We then seal the bottom of the columns with parafilm, and added 50uL 1mg/mL HA peptides (#26184, Thermo Fisher Scientific) for 15 min at 30°C with occasional mixing, and collected the elute as “HA elute1”. This step was repeated to get another 50uL HA peptide eluate as “HA elute2”. Then the beads were incubated with 50uL of 0.1M pH2.5 Glycine for 5 min at room temperature twice to get “Glycine elute 1 and 2”, which was neutralized with 5uL pH8.0 Tris. Lastly, the beads were boiled in 75uL 1*LDS loading buffer. All elutes from above were added with 25uL 3* LDS loading buffer and boiled for 5min. A small aliquot of eluted samples was resolved with SDS-PAGE, and evaluated by silver staining. Once determined the purification was successful, we loaded majority of the first HA eluates on an SDS-PAGE, stained with colloidal blue. Gel slices were excised and subsequently subjected to mass spectrometry analysis at the Harvard Taplin Mass Spectrometry facility.

Mass spectrometry and Significance analysis of INTeractome (SAINT)

Excised gel bands were cut into approximately 1 mm³ pieces. Gel pieces were then subjected to a modified in-gel trypsin digestion procedure (Shevchenko et al., 1996). Gel pieces were washed and dehydrated with acetonitrile for 10 min, followed by removal of acetonitrile. Pieces were then completely dried in a speed-vac. Rehydration of the gel pieces was with 50 mM ammonium bicarbonate solution containing 12.5 ng/μl modified sequencing-grade trypsin (Promega, Madison, WI) at 4°C. After 45 min, the excess trypsin solution was removed and replaced with 50 mM ammonium bicarbonate solution to just cover the gel pieces. Samples were then placed in a 37°C room overnight. Peptides were later extracted by removing the ammonium bicarbonate solution, followed by one wash with a solution containing 50% acetonitrile and 1% formic acid. The extracts were then dried in a speed-vac (~1 hr). The samples were then stored at 4°C until analysis.

On the day of analysis, the samples were reconstituted in 5-10 μl of HPLC solvent A (2.5% acetonitrile, 0.1% formic acid). A nano-scale reverse-phase HPLC capillary column was created by packing 2.6 μm C18 spherical silica beads into a fused silica capillary (100 μm inner diameter x ~30 cm length) with a flame-drawn tip (Peng and Gygi, 2001). After equilibrating the column each sample was loaded via a Famos auto sampler (LC Packings, San Francisco CA) onto the column. A gradient was formed and peptides were eluted with increasing concentrations of solvent B (97.5% acetonitrile, 0.1% formic acid).

Eluted peptides were subjected to electrospray ionization and then entered into an LTQ Orbitrap Velos Pro ion-trap mass spectrometer (Thermo Fisher Scientific, Waltham, MA). Peptides were detected, isolated, and fragmented to produce a tandem mass spectrum of specific fragment ions

for each peptide. Peptide sequences (and hence protein identity) were determined by matching protein databases with the acquired fragmentation pattern by the software program, Sequest (Thermo Fisher Scientific, Waltham, MA) (Eng et al., 1994). All databases include a reversed version of all the sequences and the data was filtered to between a one and two percent peptide false discovery rate.

We performed 3 biological replicates of IP-MS. Three replicates were evaluated by CRAPome (v1.1) (Contaminant Repository for Affinity Purification) analysis (<http://www.crapome.org/>) (Mellacheruvu et al., 2013). We used five HA controls with four (CC51, CC52, CC53, CC54) from CRAPome repository and one from our own HA control. To calculate SAINT scores (Choi et al., 2012), spectral counts were analyzed using SAINT parameters “Lowmode = 0, MinFold = 0, Normalize=1”. The presented SAINT score was the average probability of SAINT results from all three biological replicates. Fold change (FC) is the ratio of the normalized spectral counts of a potential HectD1-interactor to the average of three highest normalized spectral counts of that protein across the negative controls. We chose the cutoff of SAINT score ≥ 0.5 and fold change (FC) ≥ 3 based on the established HectD1-interactors (RiOK2, (Varjosalo et al., 2013); ZRANB1, (Tran et al., 2013); SMC2, (Li et al., 2015)). ZNF622 was among the top hits of all 3 replicates (Supplemental Excel). Gene Ontology (GO) analysis of HectD1-interacting proteins was performed using PANTHER Classification System (<http://pantherdb.org>) (Mi et al., 2019).

Polysome profiling

20~30 million TF-1 cells with shLuc or sh*HECTD1* were pre-treated with 100 ug/mL cycloheximide (CHX) for 5min and washed with ice-cold CHX-containing PBS. After centrifugation, cell pellets were lysed in polysome lysis buffer (20mM Tris, pH7.5, 1.5mM MgCl₂, 140mM KCl, 1% Triton X-100, 100ug/mL CHX, 0.5mM DTT, protease inhibitor cocktail) for 10min in ice with gentle rocking. The cell lysate was clarified by centrifugation at 17,000g for 10min at 4°C. OD₂₆₀ value was measured in Nanodrop. Linear sucrose gradient (7%-45%) was generated using a Gradient Maker (BioComp Instruments, Canada). 15-20 OD₂₆₀ of total cell extract was loaded on the sucrose gradient, followed by ultracentrifugation at 35,000rpm for 3hrs 20min at 4°C in SW40 rotor. Polysome profiling was analyzed with a BioComp fractionator.

For detection of protein distribution, a total of 13 fractions (830uL/fraction) from polysome profiling were collected by a fraction collector (Cat# 4422151, FC-203B, Gilson). To extract proteins for Western Blot (WB) analysis, 150uL of each fraction was pelleted by methanol-chloroform-H₂O precipitation with sequential addition of 600uL ice-cold methanol, 225uL chloroform and 450uL H₂O. The reaction was thoroughly mixed by inversion and centrifuged at 20,000g for 4min at 4°C. After carefully removing the aqueous layer, 1mL prechilled methanol was added and mixed by inversion, followed by centrifugation at 20,000g for 4min at 4°C. The supernatant was then decanted, and the protein pellet was dried at room temperature. 50uL 1* LDS loading solution was directly added to dissolve protein pellets by frequent pipetting up and down. Due to the extra abundance of proteins in cytoplasmic fractions 1-3, 2uL of fractions 1-3 along with 20uL of fractions 4-13 (different ribosomal fractions) were loaded onto an SDS-PAGE for WB analysis.

Ribosomal subunit dissociation and re-association assay

This assay was adapted from a previously published work (Burwick et al., 2012). For ribosomal subunit dissociation, 20~30 TF-1 cells were harvested without cycloheximide treatment and lysed with low Mg²⁺ buffer (20mM Tris, pH7.4, 140mM KCl, 0.25mM MgCl₂, 0.5mM DTT, 1% Triton X-100, EDTA-free protease inhibitor cocktail (Roche)) for 10min on ice. After clarification by centrifugation at 17,000g for 5min at 4°C, the cell lysate was divided into two aliquots. One aliquot

was loaded on a 7-45% low Mg^{2+} sucrose gradient (20mM Tris, pH7.4, 140mM KCl, 0.25mM $MgCl_2$, 0.5mM DTT, EDTA-free protease inhibitor cocktail (Roche)) and analyzed with a BioComp fractionator to detect total 40S and 60S.

For ribosomal subunit re-association, 2.5M $MgCl_2$ was added to the other aliquot for a final concentration of 10mM Mg^{2+} and incubated for 5min at 37°C. The resultant cell lysate was loaded on a 7-45% high Mg^{2+} sucrose gradient (20mM Tris, pH7.4, 140mM KCl, 10mM $MgCl_2$, 0.5mM DTT, EDTA-free protease inhibitor cocktail (Roche)) and analyzed with a BioComp fractionator.

Denatured His-ubiquitination assay

293T cells were transfected with indicated HectD1 and ZNF622 constructs, as well as His-tagged Ub WT, K48R or K63R mutants. 2 days later, cells were harvested and washed with cold PBS twice, and then lysed with denatured Urea Lysis buffer (100mM Na_2HPO_4 , 100mM NaH_2PO_4 , 10mM Tris, pH8.0, 0.2% Triton X-100, 5mM β -Mercaptoethanol, 10mM Imidazole, 8M urea), followed by immediate vortex and rocking at RT for 20min. After centrifuging for 10min at 15,000g, supernatant was obtained and incubated with HisPur Ni-NTA resin (88221 Thermo Scientific) for 2 hrs at RT. Resin was then washed 3 times with wash buffer (100mM Na_2HPO_4 , 100mM NaH_2PO_4 , 10mM Tris, pH6.3, 0.2% Triton X-100, 5mM β -Mercaptoethanol, 20mM Imidazole, 8M urea). Bound ubiquitinated proteins were eluted with SDS elution buffer (200mM Imidazole, 5% SDS, 150mM Tris, pH6.8, 30% glycerol, 720mM β -Mercaptoethanol) and subjected to western blot analysis.

Cytokine signaling, protein half-life assay and Western blot (WB)

For cytokine signaling, TF-1/MPL cells were starved in RPMI-1640 media plus 0.5% BSA for 2-4hrs, and then stimulated with TPO for indicated time points and snap-frozen in dry ice. For mTOR signaling, we also stimulated starved cells with a graded concentration of calf serum. Cell pellets were lysed in LDS loading buffer and sonicated for homogenization. For measuring protein half-life, cycloheximide (CHX) was employed to block de novo protein synthesis for different time points prior to cell harvest.

Protein lysates were subjected to standard WB protocols. Briefly, samples were resolved by SDS-PAGE, and transferred to NC membrane. For all primary phosphor-antibody blots, membranes were blocked with 5% BSA (BP1600-100, Fisher Bioreagents) in TBS-T, while other primary antibody blots were blocked with 5% non-fat milk (sc2325, Santa Cruz). Membranes were incubated with primary antibodies for 2hrs at room temperature or overnight in cold room. Following primary antibody blots, membranes were washed with TBS-T extensively, and then incubated with HRP-conjugated secondary antibody for 1hr at room temperature. After extensive washing, membranes were developed with ECL (#34095, Thermo Scientific). To compare immunoblots with a large number of samples that require multiple gels, samples were resolved in SDS-PAGE gels in parallel. Immunoblots were processed and developed side by side, then images were placed side-by-side for presentation.

HSC cell growth and MTT proliferation assay

100 LT-HSCs from *Hectd1^{ff}* or *Hectd1^{ff;Vav}* mice were sorted into round-bottom 96-well plate and cultured in SFEM (StemCell Technologies Inc.) supplemented with 10% FBS and various combinations or concentrations of cytokines as indicated in the main text. At different days, cell numbers were enumerated in the presence of trypan blue using a hemacytometer slide.

TF-1/MPL cells with shLuc or sh*HECTD1* were cultured in an increasing dose of GM-CSF or TPO in a 96-well plate (10k cells/100uL per well) for 3 days. 3-(4,5-dimethylthiazole-2-yl)-2,5-

diphenyl tetrazolium bromide (MTT; M6494, Invitrogen) was added to media at a final concentration of 0.5 mg/mL for 3-4 hrs at 37°C. Stopping buffer (15% SDS, 2.5% Acetic acid, 50% dimethylformamide) was then added to terminate the reaction. The absorbance was read by a spectrophotometer at 570 nm.

QUANTIFICATION AND STATISTICAL ANALYSIS

Statistics for MTT, HSC cell growth and CFC assays were performed using unpaired two-tailed Student's *t* test and error bars indicate mean± SD. Signal intensities of Western blot bands were quantified by Fiji software. Statistics was analyzed using unpaired two-tailed Student's *t* test. All the relevant quantifications performed in primary mice or transplanted mice were analyzed by GraphPad Prism and error bars indicate mean± SEM. Paired *t* test was used for pairwise comparison of HSC/MPP numbers in Cyclophosphamide+2GCSF challenged mice. Details of “n” values describing the number of experiment repeats or mice are shown in the figure legends. Statistics significance was determined by Student's *t* test. ns, not significant; *: p<0.05; **: p<0.01; ***: p<0.001.

REFERENCE

- Aleidi, S.M., Yang, A., Sharpe, L.J., Rao, G., Cochran, B.J., Rye, K.A., Kockx, M., Brown, A.J., and Gelissen, I.C. (2018). The E3 ubiquitin ligase, HECTD1, is involved in ABCA1-mediated cholesterol export from macrophages. *Biochim Biophys Acta Mol Cell Biol Lipids* 1863, 359-368.
- Balcerek, J., Jiang, J., Li, Y., Jiang, Q., Holdreith, N., Singh, B., Chandra, V., Lv, K., Ren, J.G., Rozenova, K., *et al.* (2018). Lnk/Sh2b3 deficiency restores hematopoietic stem cell function and genome integrity in Fancd2 deficient Fanconi anemia. *Nat Commun* 9, 3915.
- Barilari, M., Bonfils, G., Treins, C., Koka, V., De Villeneuve, D., Fabrega, S., and Pende, M. (2017). ZRF1 is a novel S6 kinase substrate that drives the senescence programme. *EMBO J* 36, 736-750.
- Bersenev, A., Wu, C., Balcerek, J., and Tong, W. (2008). Lnk controls mouse hematopoietic stem cell self-renewal and quiescence through direct interactions with JAK2. *J Clin Invest* 118, 2832-2844.
- Boocock, G.R., Morrison, J.A., Popovic, M., Richards, N., Ellis, L., Durie, P.R., and Rommens, J.M. (2003). Mutations in SBDS are associated with Shwachman-Diamond syndrome. *Nat Genet* 33, 97-101.
- Burwick, N., Coats, S.A., Nakamura, T., and Shimamura, A. (2012). Impaired ribosomal subunit association in Shwachman-Diamond syndrome. *Blood* 120, 5143-5152.
- Chauvin, C., Koka, V., Nouschi, A., Mieulet, V., Hoareau-Aveilla, C., Dreazen, A., Cagnard, N., Carpentier, W., Kiss, T., Meyuhas, O., *et al.* (2014). Ribosomal protein S6 kinase activity controls the ribosome biogenesis transcriptional program. *Oncogene* 33, 474-483.
- Chen, M.J., Yokomizo, T., Zeigler, B.M., Dzierzak, E., and Speck, N.A. (2009). Runx1 is required for the endothelial to haematopoietic cell transition but not thereafter. *Nature* 457, 887-891.
- Choi, H., Liu, G., Mellacheruvu, D., Tyers, M., Gingras, A.C., and Nesvizhskii, A.I. (2012). Analyzing protein-protein interactions from affinity purification-mass spectrometry data with SAINT. *Curr Protoc Bioinformatics Chapter* 8, Unit8 15.
- D'Alonzo, D., Emch, F.H., Shen, X., Bruder, E., De Geyter, C., and Zhang, H. (2019). Hectd1 is essential for embryogenesis in mice. *Gene Expr Patterns* 34, 119064.
- de la Cruz, J., Karbstein, K., and Woolford, J.L., Jr. (2015). Functions of ribosomal proteins in assembly of eukaryotic ribosomes in vivo. *Annu Rev Biochem* 84, 93-129.
- Dhanraj, S., Matveev, A., Li, H., Lauhasurayotin, S., Jardine, L., Cada, M., Zlateska, B., Tailor, C.S., Zhou, J., Mendoza-Londono, R., *et al.* (2017). Biallelic mutations in DNAJC21 cause Shwachman-Diamond syndrome. *Blood* 129, 1557-1562.
- Duhamel, S., Goyette, M.A., Thibault, M.P., Filion, D., Gaboury, L., and Cote, J.F. (2018). The E3 Ubiquitin Ligase HectD1 Suppresses EMT and Metastasis by Targeting the +TIP ACF7 for Degradation. *Cell Rep* 22, 1016-1030.
- Eng, J.K., McCormack, A.L., and Yates, J.R. (1994). An approach to correlate tandem mass spectral data of peptides with amino acid sequences in a protein database. *J Am Soc Mass Spectrom* 5, 976-989.
- Finch, A.J., Hilcenko, C., Basse, N., Drynan, L.F., Goyenechea, B., Menne, T.F., Gonzalez Fernandez, A., Simpson, P., D'Santos, C.S., Arends, M.J., *et al.* (2011). Uncoupling of GTP hydrolysis from eIF6 release on the ribosome causes Shwachman-Diamond syndrome. *Genes Dev* 25, 917-929.
- Greber, B.J., Boehringer, D., Montellese, C., and Ban, N. (2012). Cryo-EM structures of Arx1 and maturation factors Rei1 and Jjj1 bound to the 60S ribosomal subunit. *Nat Struct Mol Biol* 19, 1228-1233.

Greber, B.J., Gerhardy, S., Leitner, A., Leibundgut, M., Salem, M., Boehringer, D., Leulliot, N., Aebersold, R., Panse, V.G., and Ban, N. (2016). Insertion of the Biogenesis Factor Rei1 Probes the Ribosomal Tunnel during 60S Maturation. *Cell* *164*, 91-102.

Holcik, M., and Sonenberg, N. (2005). Translational control in stress and apoptosis. *Nat Rev Mol Cell Biol* *6*, 318-327.

Hu, Y., and Smyth, G.K. (2009). ELDA: extreme limiting dilution analysis for comparing depleted and enriched populations in stem cell and other assays. *J Immunol Methods* *347*, 70-78.

Jiang, J., Balcerek, J., Rozenova, K., Cheng, Y., Bersenev, A., Wu, C., Song, Y., and Tong, W. (2012). 14-3-3 regulates the LNK/JAK2 pathway in mouse hematopoietic stem and progenitor cells. *J Clin Invest* *122*, 2079-2091.

Kargas, V., Castro-Hartmann, P., Escudero-Urquijo, N., Dent, K., Hilcenko, C., Sailer, C., Zisser, G., Marques-Carvalho, M.J., Pellegrino, S., Wawiora, L., *et al.* (2019). Mechanism of completion of peptidyltransferase centre assembly in eukaryotes. *Elife* *8*.

Kisly, I., Remme, J., and Tamm, T. (2019). Ribosomal protein eL24, involved in two intersubunit bridges, stimulates translation initiation and elongation. *Nucleic Acids Res* *47*, 406-420.

Klinge, S., and Woolford, J.L., Jr. (2019). Ribosome assembly coming into focus. *Nat Rev Mol Cell Biol* *20*, 116-131.

Li, W., Hu, Y., Oh, S., Ma, Q., Merkurjev, D., Song, X., Zhou, X., Liu, Z., Tanasa, B., He, X., *et al.* (2015). Condensin I and II Complexes License Full Estrogen Receptor alpha-Dependent Enhancer Activation. *Mol Cell* *59*, 188-202.

Liaud, N., Horlbeck, M.A., Gilbert, L.A., Gjoni, K., Weissman, J.S., and Cate, J.H.D. (2019). Cellular response to small molecules that selectively stall protein synthesis by the ribosome. *PLoS Genet* *15*, e1008057.

Liu, J., Xu, Y., Stoleru, D., and Salic, A. (2012). Imaging protein synthesis in cells and tissues with an alkyne analog of puromycin. *Proc Natl Acad Sci U S A* *109*, 413-418.

Lo, K.Y., Li, Z., Bussiere, C., Bresson, S., Marcotte, E.M., and Johnson, A.W. (2010). Defining the pathway of cytoplasmic maturation of the 60S ribosomal subunit. *Mol Cell* *39*, 196-208.

Lv, K., Jiang, J., Donaghy, R., Riling, C.R., Cheng, Y., Chandra, V., Rozenova, K., An, W., Mohapatra, B.C., Goetz, B.T., *et al.* (2017). CBL family E3 ubiquitin ligases control JAK2 ubiquitination and stability in hematopoietic stem cells and myeloid malignancies. *Genes Dev* *31*, 1007-1023.

Ma, C., Wu, S., Li, N., Chen, Y., Yan, K., Li, Z., Zheng, L., Lei, J., Woolford, J.L., Jr., and Gao, N. (2017). Structural snapshot of cytoplasmic pre-60S ribosomal particles bound by Nmd3, Lsg1, Tif6 and Reh1. *Nat Struct Mol Biol* *24*, 214-220.

Mellacheruvu, D., Wright, Z., Couzens, A.L., Lambert, J.P., St-Denis, N.A., Li, T., Miteva, Y.V., Hauri, S., Sardi, M.E., Low, T.Y., *et al.* (2013). The CRAPome: a contaminant repository for affinity purification-mass spectrometry data. *Nat Methods* *10*, 730-736.

Menne, T.F., Goyenechea, B., Sanchez-Puig, N., Wong, C.C., Tonkin, L.M., Ancliff, P.J., Brost, R.L., Costanzo, M., Boone, C., and Warren, A.J. (2007). The Shwachman-Bodian-Diamond syndrome protein mediates translational activation of ribosomes in yeast. *Nat Genet* *39*, 486-495.

Meyer, A.E., Hoover, L.A., and Craig, E.A. (2010). The cytosolic J-protein, Jjj1, and Rei1 function in the removal of the pre-60 S subunit factor Arx1. *J Biol Chem* *285*, 961-968.

Mi, H., Muruganujan, A., Ebert, D., Huang, X., and Thomas, P.D. (2019). PANTHER version 14: more genomes, a new PANTHER GO-slim and improvements in enrichment analysis tools. *Nucleic Acids Res* *47*, D419-D426.

Modlich, U., Schambach, A., Li, Z., and Schiedlmeier, B. (2009). Murine hematopoietic stem cell transduction using retroviral vectors. *Methods Mol Biol* *506*, 23-31.

Morrison, S.J., Wright, D.E., and Weissman, I.L. (1997). Cyclophosphamide/granulocyte colony-stimulating factor induces hematopoietic stem cells to proliferate prior to mobilization. *Proc Natl Acad Sci U S A* *94*, 1908-1913.

Oguro, H., Ding, L., and Morrison, S.J. (2013). SLAM family markers resolve functionally distinct subpopulations of hematopoietic stem cells and multipotent progenitors. *Cell Stem Cell* *13*, 102-116.

Peng, J., and Gygi, S.P. (2001). Proteomics: the move to mixtures. *J Mass Spectrom* *36*, 1083-1091.

Pietras, E.M., Reynaud, D., Kang, Y.A., Carlin, D., Calero-Nieto, F.J., Leavitt, A.D., Stuart, J.M., Gottgens, B., and Passegue, E. (2015). Functionally Distinct Subsets of Lineage-Biased Multipotent Progenitors Control Blood Production in Normal and Regenerative Conditions. *Cell Stem Cell* *17*, 35-46.

Rodriguez, C.I., Buchholz, F., Galloway, J., Sequerra, R., Kasper, J., Ayala, R., Stewart, A.F., and Dymecki, S.M. (2000). High-efficiency deleter mice show that FLPe is an alternative to Cre-loxP. *Nat Genet* *25*, 139-140.

Rozenova, K., Jiang, J., Donaghy, R., Aressy, B., Greenberg, R.A., and Tong, W. (2015). MERIT40 deficiency expands hematopoietic stem cell pools by regulating thrombopoietin receptor signaling. *Blood* *125*, 1730-1738.

Ruggero, D., and Shimamura, A. (2014). Marrow failure: a window into ribosome biology. *Blood* *124*, 2784-2792.

Sarkar, A.A., Nuwayhid, S.J., Maynard, T., Ghandchi, F., Hill, J.T., Lamantia, A.S., and Zohn, I.E. (2014). Hectd1 is required for development of the junctional zone of the placenta. *Dev Biol* *392*, 368-380.

Sarkar, A.A., and Zohn, I.E. (2012). Hectd1 regulates intracellular localization and secretion of Hsp90 to control cellular behavior of the cranial mesenchyme. *J Cell Biol* *196*, 789-800.

Shembade, N., and Harhaj, E.W. (2015). Elucidating dynamic protein-protein interactions and ubiquitination in NF-kappaB signaling pathways. *Methods Mol Biol* *1280*, 283-295.

Shevchenko, A., Wilm, M., Vorm, O., and Mann, M. (1996). Mass spectrometric sequencing of proteins silver-stained polyacrylamide gels. *Anal Chem* *68*, 850-858.

Signer, R.A., Magee, J.A., Salic, A., and Morrison, S.J. (2014). Haematopoietic stem cells require a highly regulated protein synthesis rate. *Nature* *509*, 49-54.

Signer, R.A., Qi, L., Zhao, Z., Thompson, D., Sigova, A.A., Fan, Z.P., DeMartino, G.N., Young, R.A., Sonenberg, N., and Morrison, S.J. (2016). The rate of protein synthesis in hematopoietic stem cells is limited partly by 4E-BPs. *Genes Dev* *30*, 1698-1703.

Stadtfeld, M., and Graf, T. (2005). Assessing the role of hematopoietic plasticity for endothelial and hepatocyte development by non-invasive lineage tracing. *Development* *132*, 203-213.

Sugrue, K.F., Sarkar, A.A., Leatherbury, L., and Zohn, I.E. (2019). The ubiquitin ligase HECTD1 promotes retinoic acid signaling required for development of the aortic arch. *Dis Model Mech* *12*.

Sulima, S.O., Hofman, I.J.F., De Keersmaecker, K., and Dinman, J.D. (2017). How Ribosomes Translate Cancer. *Cancer Discov* *7*, 1069-1087.

Tan, S., Kermasson, L., Hoslin, A., Jaako, P., Faille, A., Acevedo-Arozena, A., Lengline, E., Ranta, D., Poiree, M., Fenneteau, O., *et al.* (2019). EFL1 mutations impair eIF6 release to cause Shwachman-Diamond syndrome. *Blood* *134*, 277-290.

Tran, H., Bustos, D., Yeh, R., Rubinfeld, B., Lam, C., Shriver, S., Zilberleyb, I., Lee, M.W., Phu, L., Sarkar, A.A., *et al.* (2013). HectD1 E3 ligase modifies adenomatous polyposis coli (APC) with polyubiquitin to promote the APC-axin interaction. *J Biol Chem* *288*, 3753-3767.

Tummala, H., Walne, A.J., Williams, M., Bockett, N., Collopy, L., Cardoso, S., Ellison, A., Wynn, R., Leblanc, T., Fitzgibbon, J., *et al.* (2016). DNAJC21 Mutations Link a Cancer-Prone

Bone Marrow Failure Syndrome to Corruption in 60S Ribosome Subunit Maturation. *Am J Hum Genet* 99, 115-124.

Warren, A.J. (2018). Molecular basis of the human ribosomopathy Shwachman-Diamond syndrome. *Advances in biological regulation* 67, 109-127.

Weis, F., Giudice, E., Churcher, M., Jin, L., Hilcenko, C., Wong, C.C., Traynor, D., Kay, R.R., and Warren, A.J. (2015). Mechanism of eIF6 release from the nascent 60S ribosomal subunit. *Nat Struct Mol Biol* 22, 914-919.

Wilson, A., Laurenti, E., Oser, G., van der Wath, R.C., Blanco-Bose, W., Jaworski, M., Offner, S., Dunant, C.F., Eshkind, L., Bockamp, E., *et al.* (2008). Hematopoietic stem cells reversibly switch from dormancy to self-renewal during homeostasis and repair. *Cell* 135, 1118-1129.

Woloszynek, J.R., Rothbaum, R.J., Rawls, A.S., Minx, P.J., Wilson, R.K., Mason, P.J., Bessler, M., and Link, D.C. (2004). Mutations of the SBDS gene are present in most patients with Shwachman-Diamond syndrome. *Blood* 104, 3588-3590.

Wong, C.C., Traynor, D., Basse, N., Kay, R.R., and Warren, A.J. (2011). Defective ribosome assembly in Shwachman-Diamond syndrome. *Blood* 118, 4305-4312.

Zohn, I.E., Anderson, K.V., and Niswander, L. (2007). The Hectd1 ubiquitin ligase is required for development of the head mesenchyme and neural tube closure. *Dev Biol* 306, 208-221.

Figure 1. Lv, et al

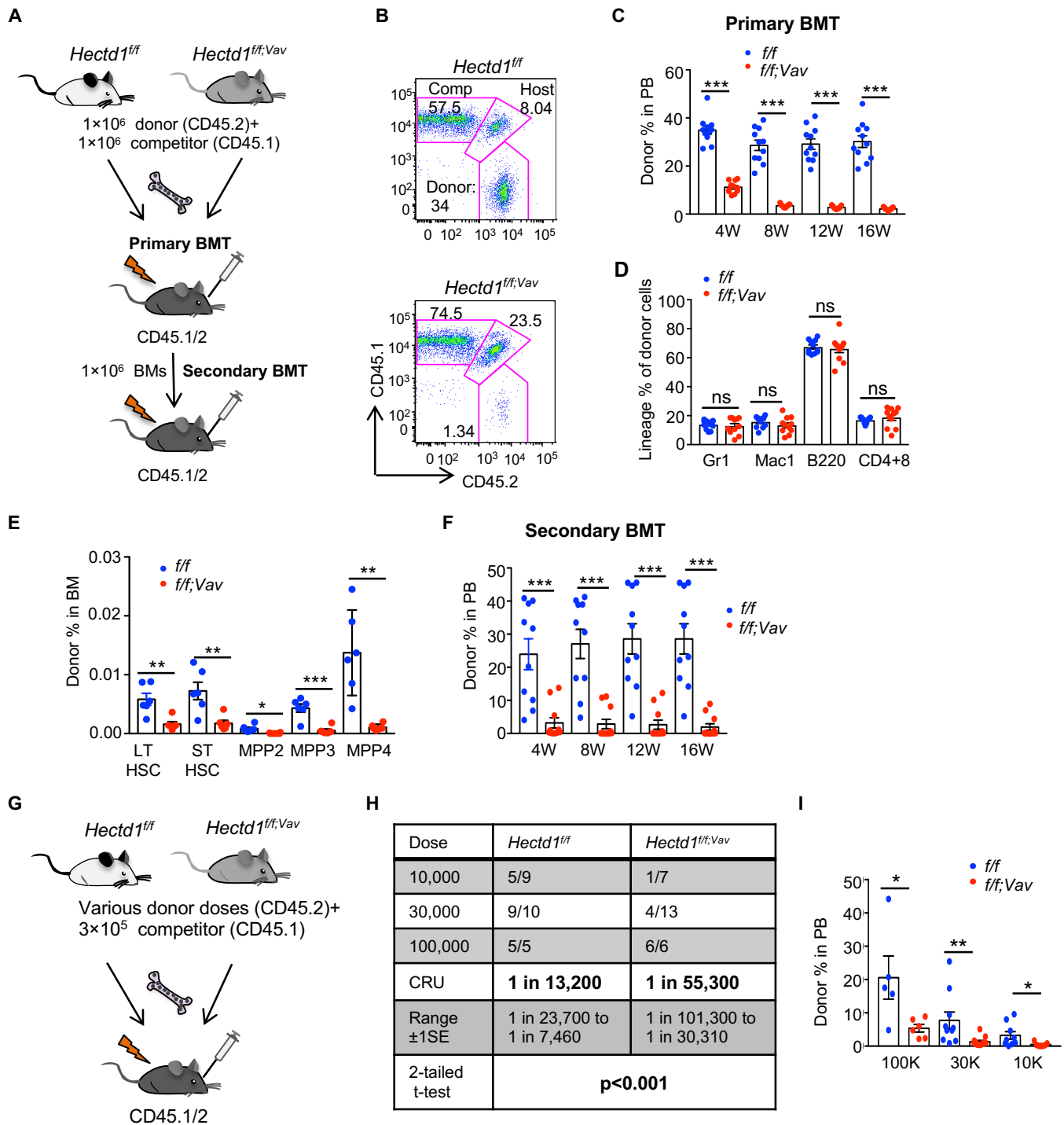


Figure 2. Lv, et al (smaller size)

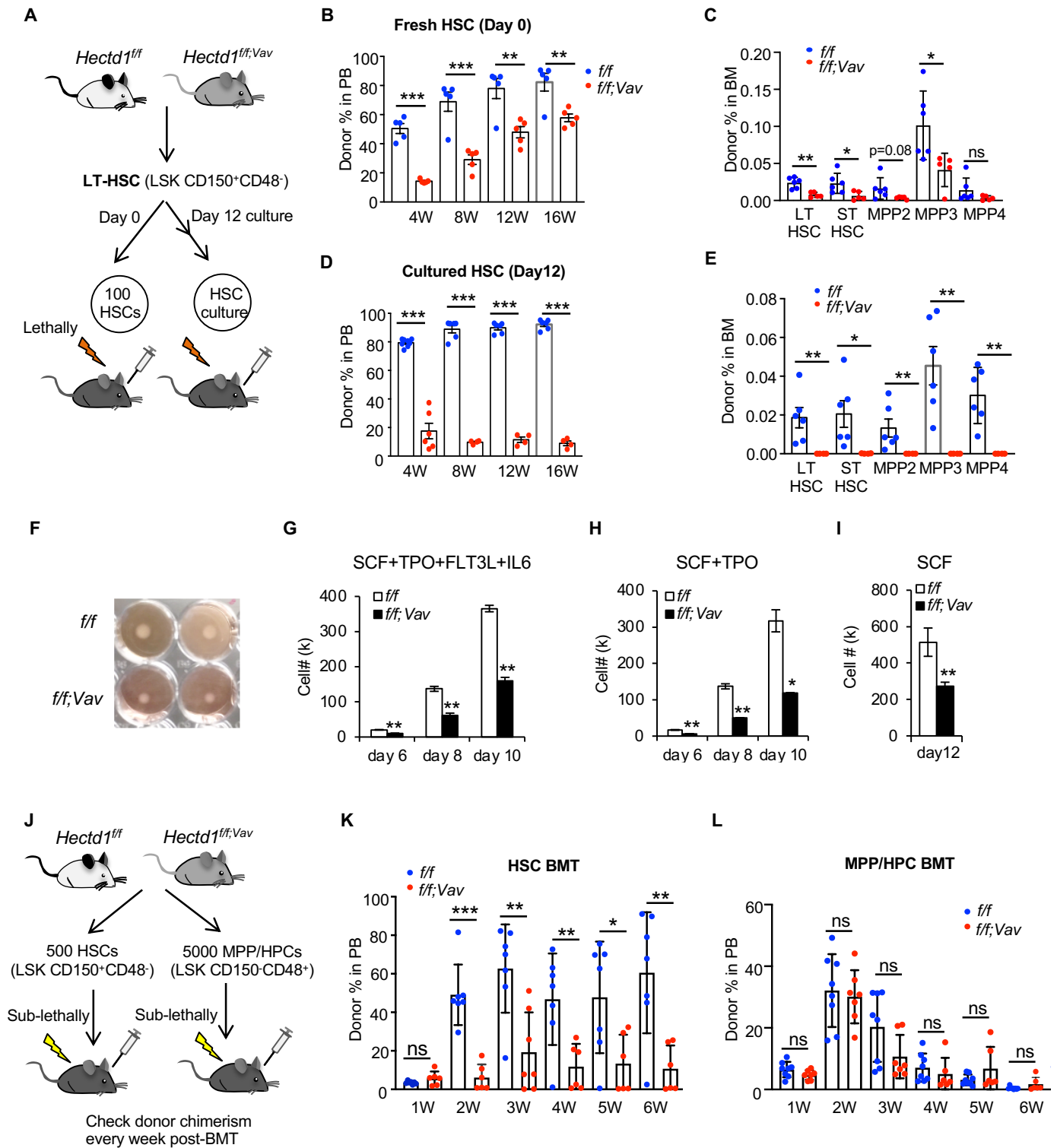


Figure 3. Lv, et al (smaller size)

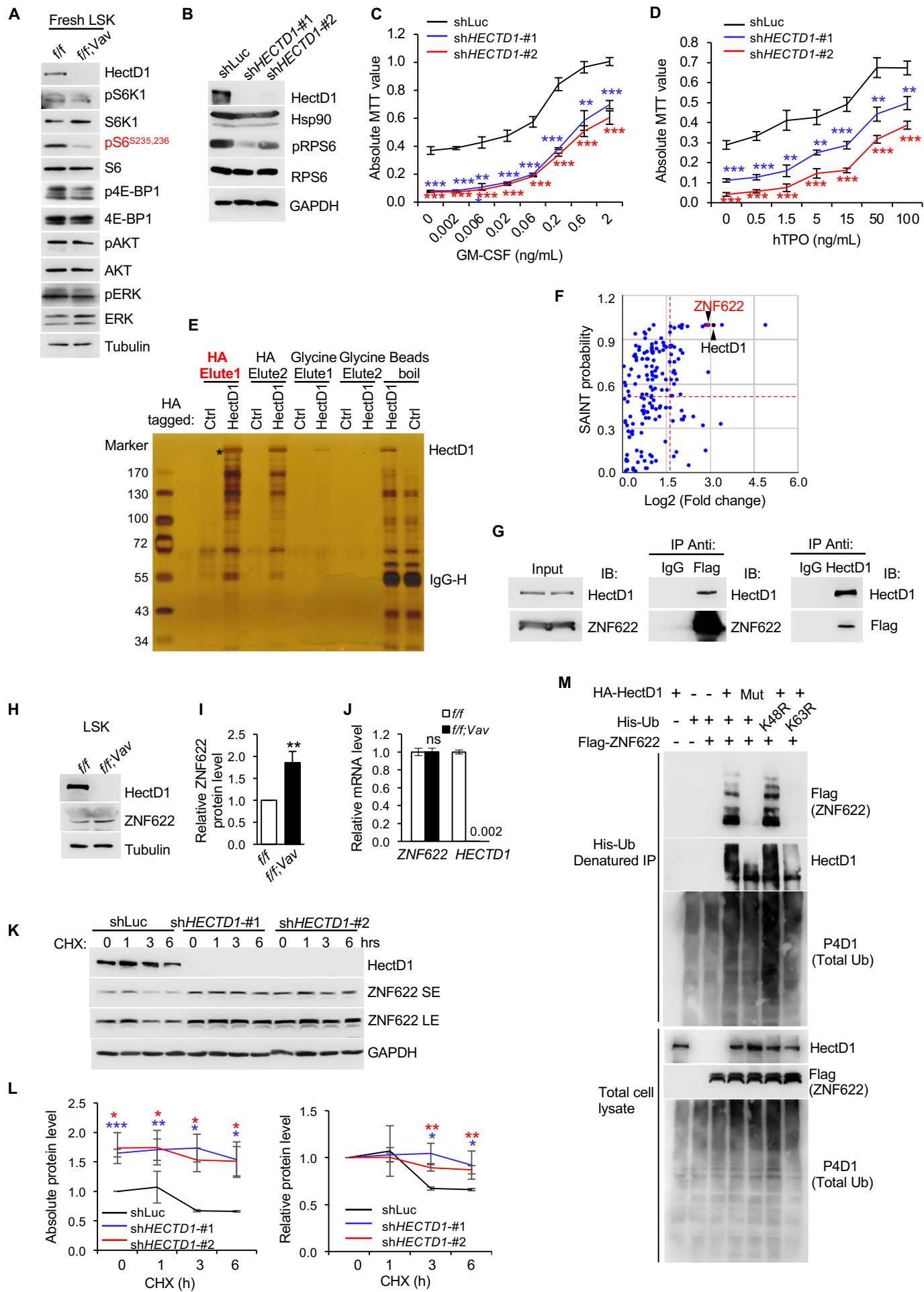


Figure 4. Lv, et al

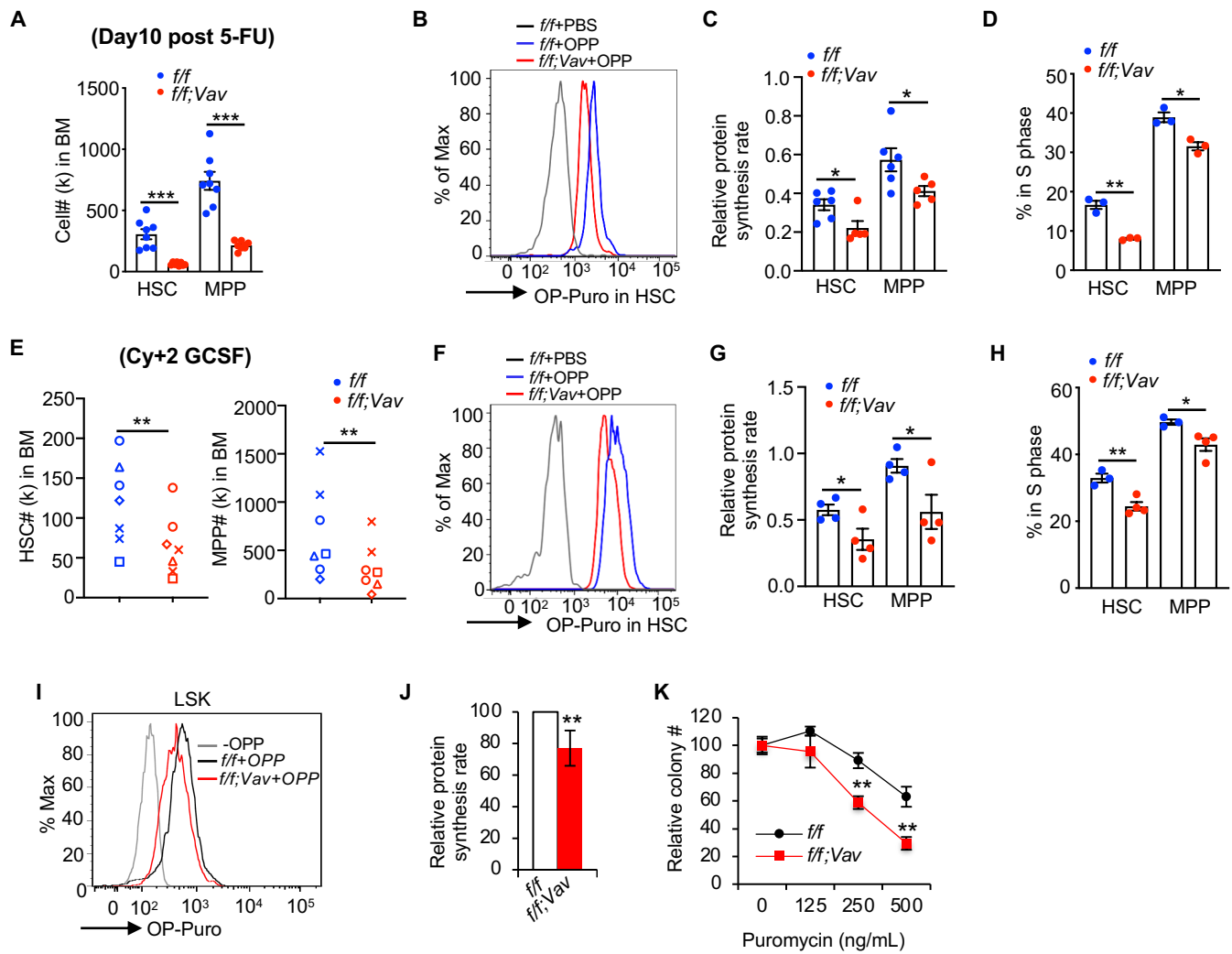


Figure 5. Lv, et al

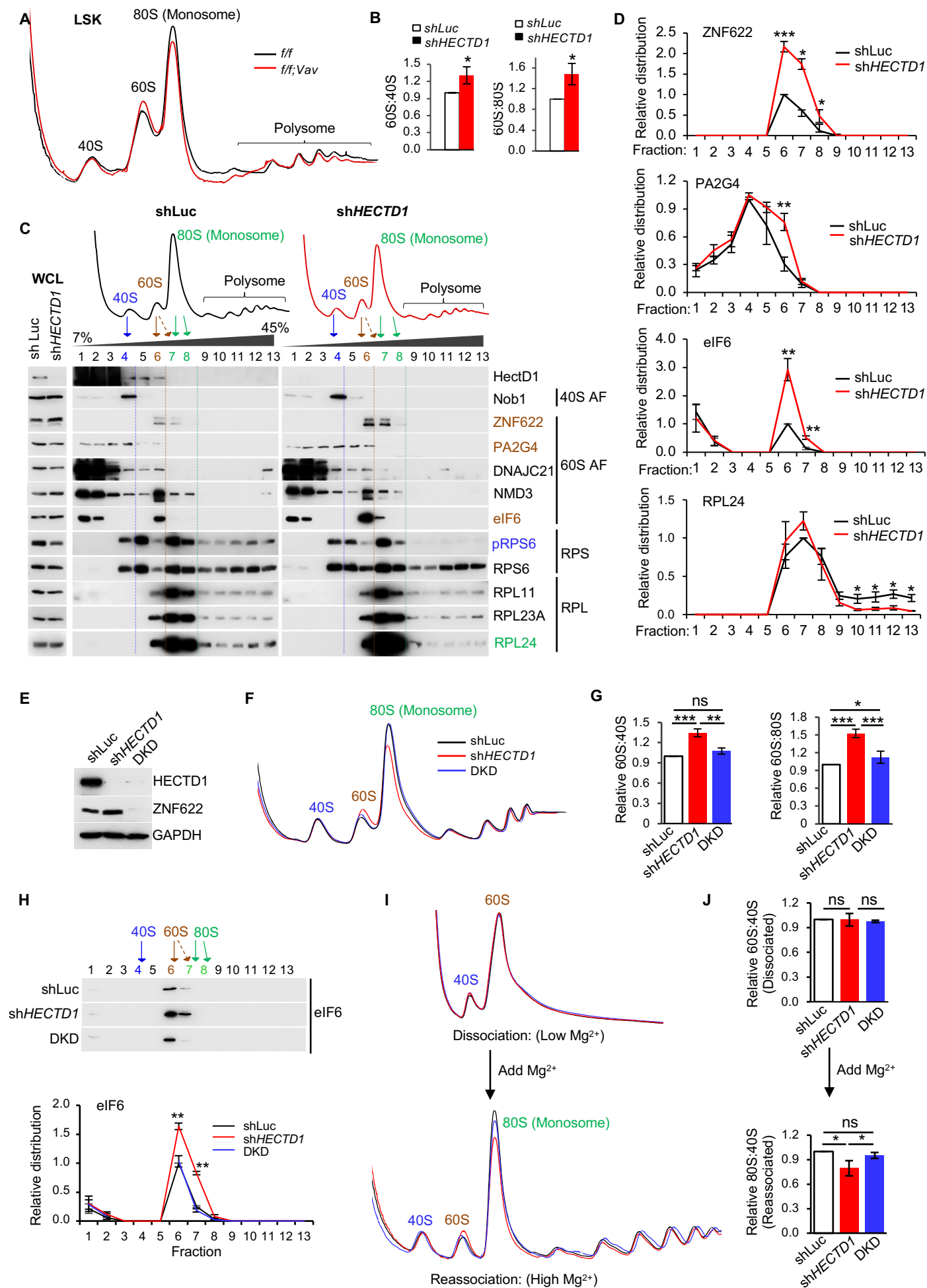
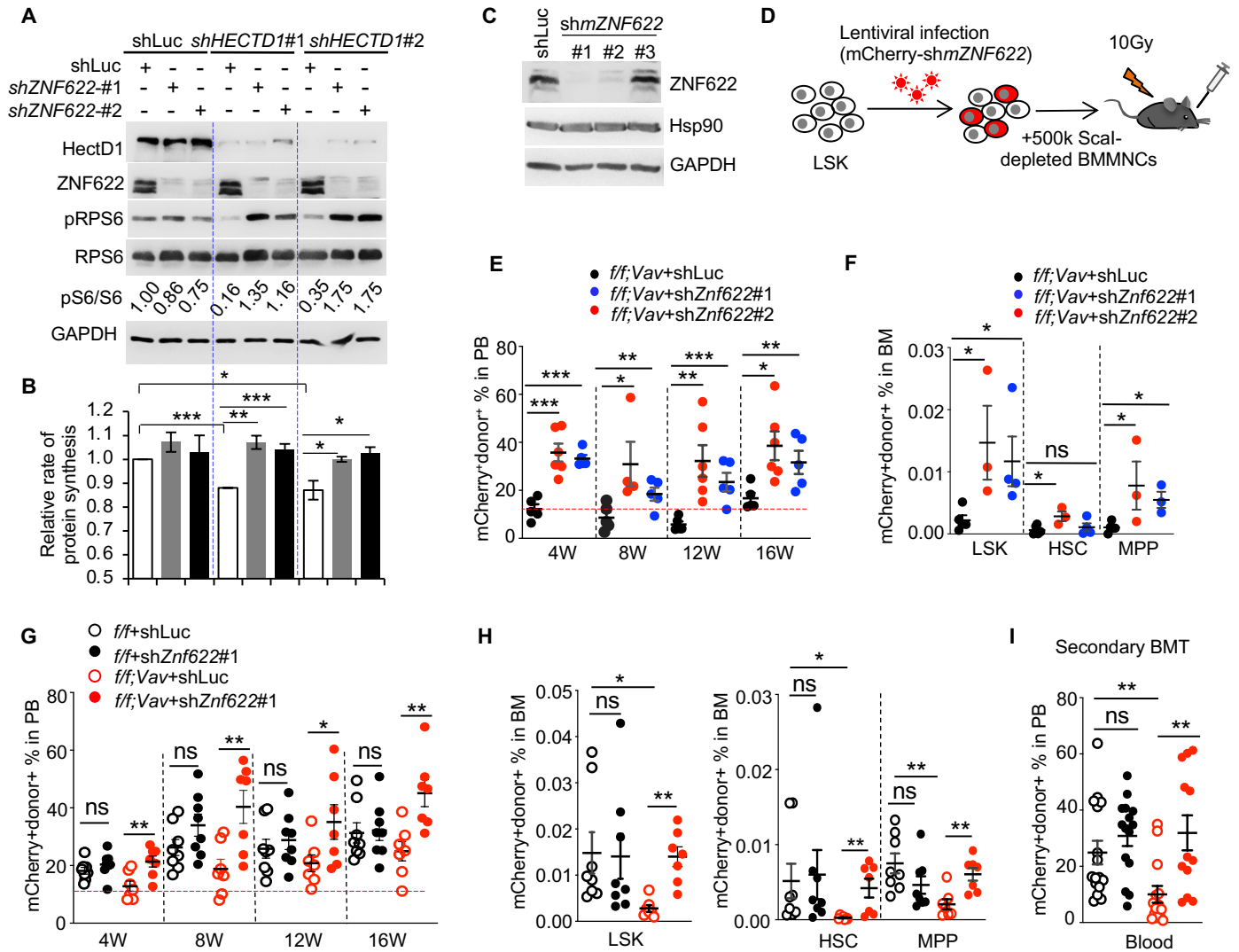


Figure 6. Lv, et al



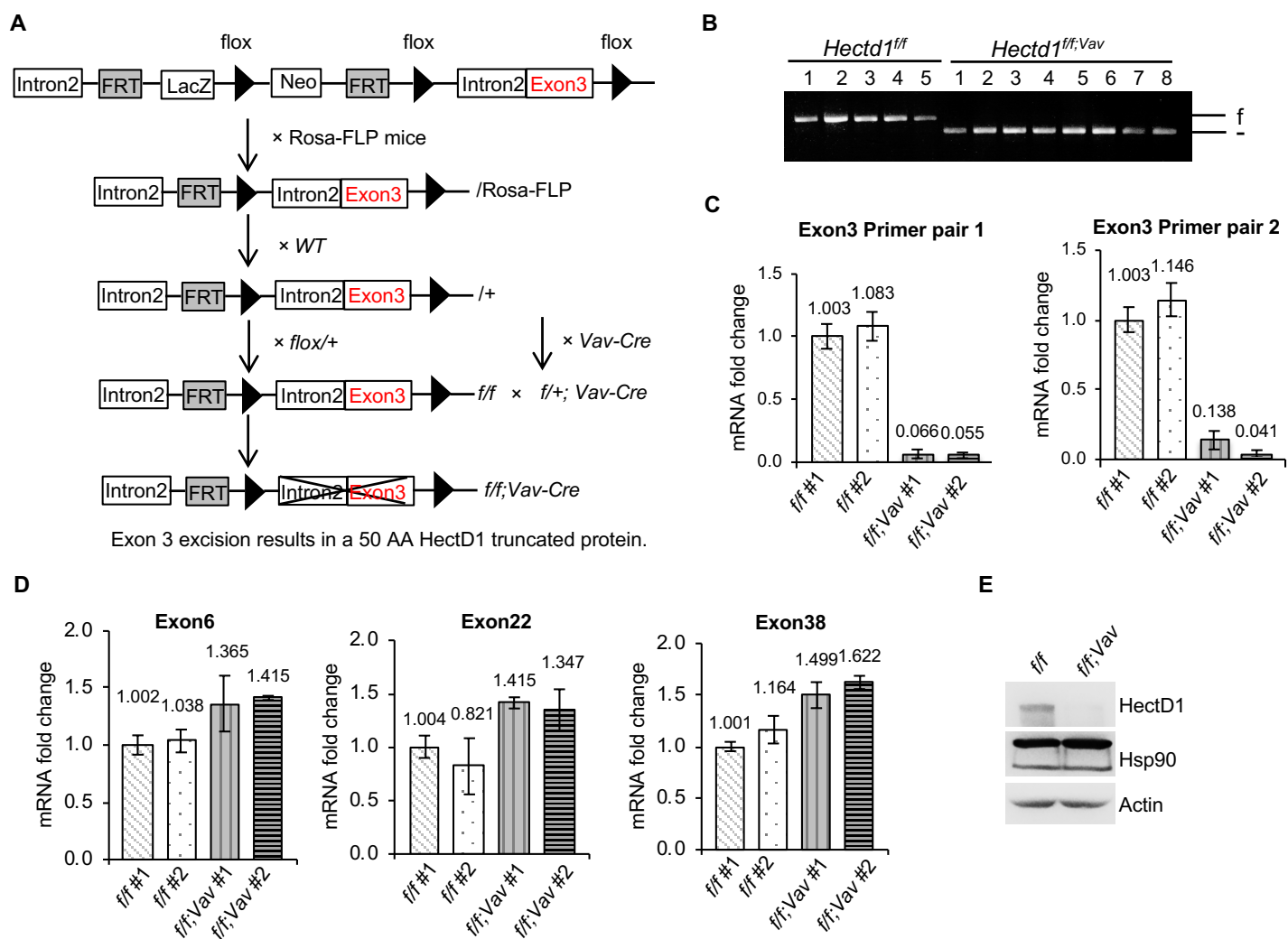


Figure S1. Generation of hematopoietic-specific *Hectd1* conditional knockout mice. Related to Figure 1.

(A) Strategy of generating Vav-cre mediated conditional *Hectd1* knockout (*Hectd1*^{f/f;Vav}) mice. Exon3 was flanked by floxP sites. Deletion of exon 3 results in an early stop codon in exon4, producing a 50 aa (amino acid) truncated protein.

(B) Genotyping of individual bone marrow-derived hematopoietic colonies from *Hectd1*^{f/f} and *Hectd1*^{f/f;Vav} mice to evaluate *Hectd1* deletion efficiency.

(C) RT-qPCR analysis to evaluate the deletion efficiency of *Hectd1* at the mRNA level. *Hectd1* contains 43 exons. qPCR primer pairs targeting to exon 3 are designed and used for qPCR analysis. BM cells from two mice of each genotype were tested.

(D) As negative controls, qPCR primer pairs targeted to *Hectd1* exon 6, 22, 38 were designed and used to confirm the specificity of *Hectd1* excision in mice.

(E) Western blot analysis of BM cells to confirm *Hectd1* knockout efficiency at the protein level. Data are represented by mean± SD in (C, D).

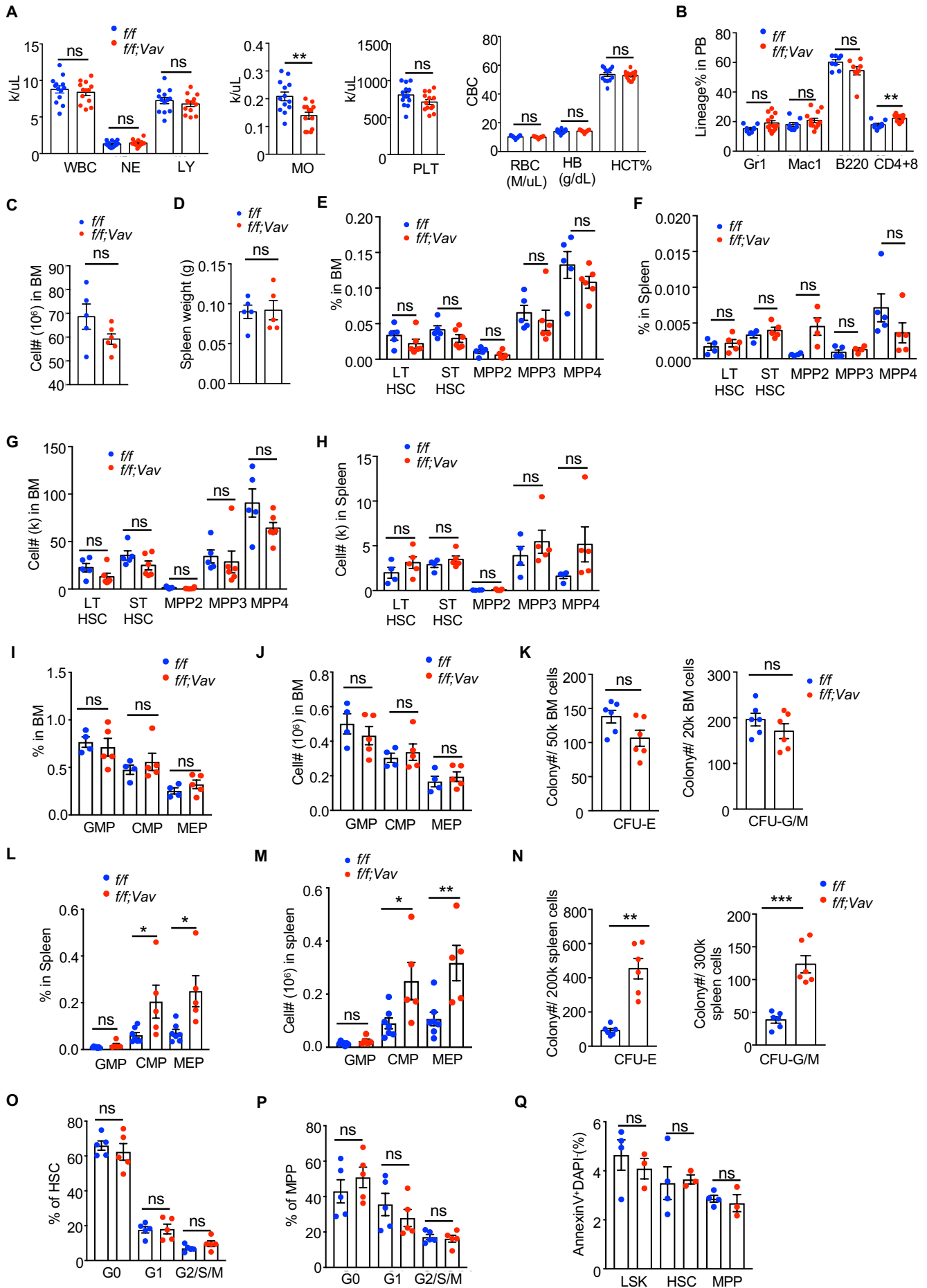


Figure S2. Hematopoietic-specific *Hectd1* knockout mice show relatively normal steady-state hematopoiesis. Related to Figure 1.

(A) Complete blood count (CBC) analysis of peripheral blood (PB) from *Hectd1^{ff}* (n=13) and *Hectd1^{ff;Vav}* (n=13) mice. WBC, whole blood count; NE, neutrophils; LY, lymphocytes; MO, monocytes; PLT, platelets; RBC, red blood cells; HB, hemoglobin; HCT, hematocrit.

(B) Lineage cell percentages in the PB of *Hectd1^{ff}* (n=8) and *Hectd1^{ff;Vav}* (n=11) mice were analyzed by flow cytometry.

(C) Total BM cellularity of *Hectd1^{ff}* (n=5) and *Hectd1^{ff;Vav}* (n=6) mice.

(D) Spleen weight of *Hectd1^{ff}* (n=5) and *Hectd1^{ff;Vav}* (n=5) mice.

(E, F) Flow cytometry analysis of the frequency of various HSPC subpopulations in BM (E) and spleen (F) of *Hectd1^{ff}* (n=5) and *Hectd1^{ff;Vav}* (n=6) mice. Long-term hematopoietic stem cell (LT-HSC) is defined as CD150⁺CD48⁻Flk2⁻LSK cells. Short-term HSC (ST-HSC): CD150⁻CD48⁻Flk2⁻LSK. MPP2: CD150⁺CD48⁺Flk2⁻LSK. MPP3: CD150⁻CD48⁺Flk2⁻LSK. MPP4: CD150⁻Flk2⁺LSK.

(G-H) Cell numbers of HSPC subpopulations in BM (G) and spleen (H) of *Hectd1^{ff}* (n=5) and *Hectd1^{ff;Vav}* (n=5) mice.

(I, J) Frequency (I) and cell number (J) of different hematopoietic progenitors in BM of *Hectd1^{ff}* (n=5) and *Hectd1^{ff;Vav}* (n=6) mice as determined by flow cytometry are shown.

(K) Colony-forming units (CFU)-E (left) and CFU-G/M (right) of the BM are shown.

(L, M), Frequency (L) and cell number (M) of different hematopoietic progenitors in the spleen of *Hectd1^{ff}* (n=5) and *Hectd1^{ff;Vav}* (n=6) mice are shown.

(N) CFU-E (left) and CFU-G/M (right) analysis of the spleen are shown.

(O-P) Cell cycle analysis of HSCs (O) and MPPs (P) in primary *Hectd1^{ff}* (n=5) and *Hectd1^{ff;Vav}* (n=5) mice as determined by Ki67 and DAPI.

(Q) Cell apoptosis analysis of LSKs, HSCs and MPPs in primary *Hectd1^{ff}* (n=4) and *Hectd1^{ff;Vav}* (n=3) mice by Annexin V staining.

All the experiments above were performed in 8-10 weeks old young mice. Each symbol represents an individual mouse; bars indicate mean values; error bars indicate SE. *: p<0.05; **: p<0.01; ***: p<0.001; ns: not significant, as determined by two-tailed Student's *t*-tests.

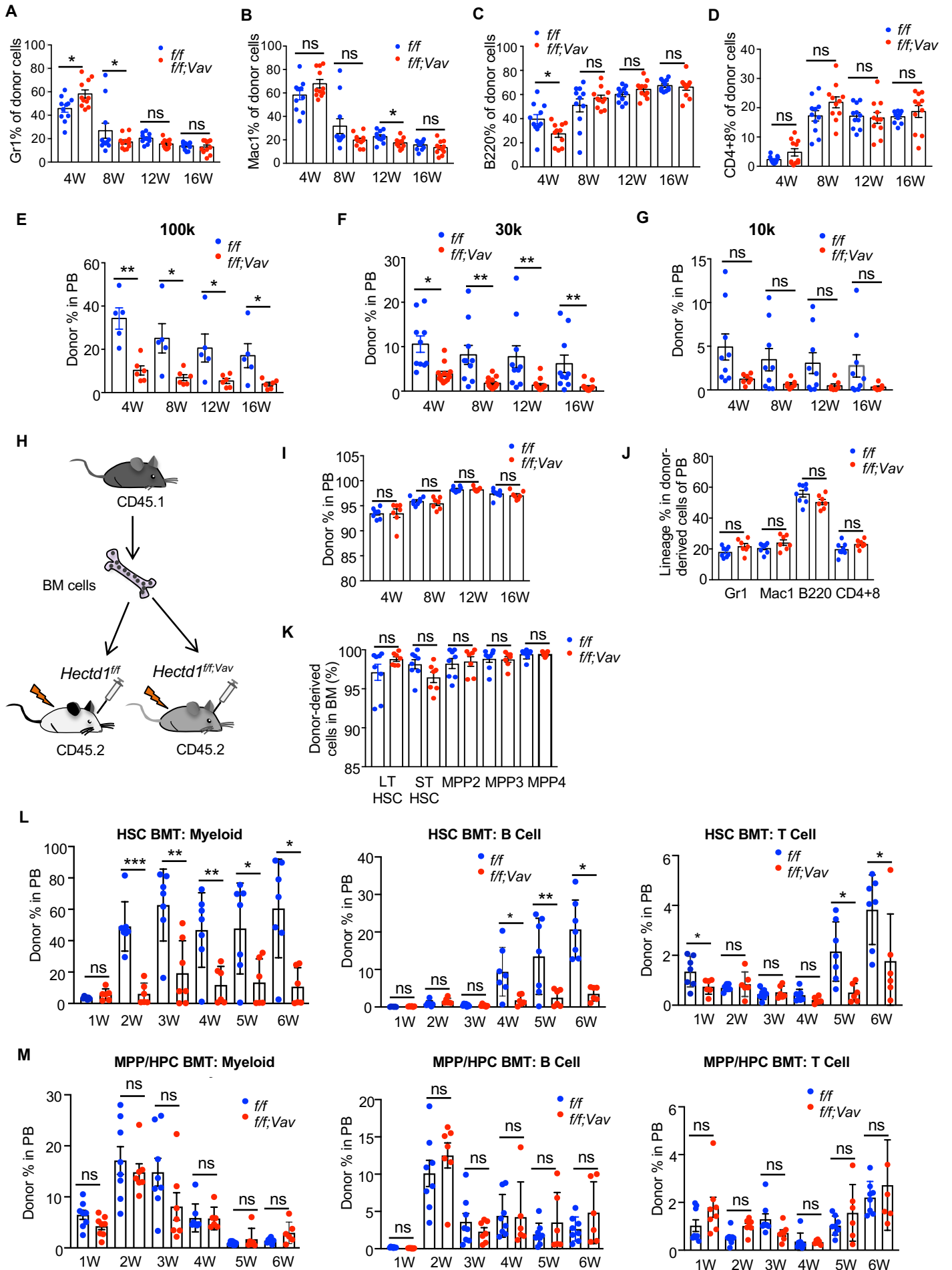


Figure S3. Loss of *Hectd1* does not impair hematopoietic differentiation, bone marrow niche or MPP reconstitution in transplanted mice. Panels S3A-S3K are related to figure 1 and panels S3L-S3M are related to figure 2.

(A-D) Loss of *Hectd1* does not impair hematopoietic differentiation in transplanted mice. Examination of donor HSC differentiation in competitive total BM transplanted mice. 1×10^6 unfractionated BM cells from *Hectd1^{ff}* and *Hectd1^{ff;Vav}* mice were injected with the same number of competitor BM cells into lethally irradiated recipient mice. Donor chimerisms in different lineages of the PB were shown. (A) Granulocytes, (B) monocytes, (C) B cells and (D) T cells. *Hectd1^{ff}* (n=11) and *Hectd1^{ff;Vav}* (n=11).

(E-G) *Hectd1* deficiency leads to a decreased donor reconstitution in limiting dilution BMT. Donor cell percentage in recipients' PB injected with 100k (E), 30k (F), 10k (G) donor BM cells mixed with 300k competitor BM cells were examined every 4 weeks post-BMT. 100k: *Hectd1^{ff}* (n=5) and *Hectd1^{ff;Vav}* (n=6); 30k: *Hectd1^{ff}* (n=10) and *Hectd1^{ff;Vav}* (n=13); 10k: *Hectd1^{ff}* (n=9) and *Hectd1^{ff;Vav}* (n=7).

(H-K) *Hectd1* deficiency does not affect bone marrow niche as shown in reciprocal BMT.

(H) Experimental scheme of reciprocal BMT. 1×10^6 total BM cells from SJL mice (CD45.1) were transplanted into lethally irradiated *Hectd1^{ff}* (n=8) and *Hectd1^{ff;Vav}* (n=7) littermates (CD45.2).

(I) Donor chimerism was analyzed by flow cytometry every 4 weeks post-BMT.

(J) Donor-derived cells in each lineage 16 weeks post-BMT are shown.

(K) Donor percentages in different HSPC subpopulations in the BM of *Hectd1^{ff}* and *Hectd1^{ff;Vav}* recipient mice are shown.

(L-M) *Hectd1* is required for HSC but not MPP/HPC reconstitution ability.

(L) Percentages of donor HSC-derived myeloid cells (Gr1/Mac1⁺), B cells (B220⁺) and T cells (CD4⁺CD8⁺) are shown.

(M) Percentages of donor MPP/HPC-derived myeloid cells (Gr1/Mac1⁺), B cells (B220⁺) and T cells (CD4⁺CD8⁺) are shown.

In all relevant panels, each symbol represents an individual mouse; bars indicate mean frequencies; error bars indicate SE.

*: p<0.05; **: p<0.01; ***: p<0.001; ns, not significant, as determined by two-tailed Student's *t*-tests.

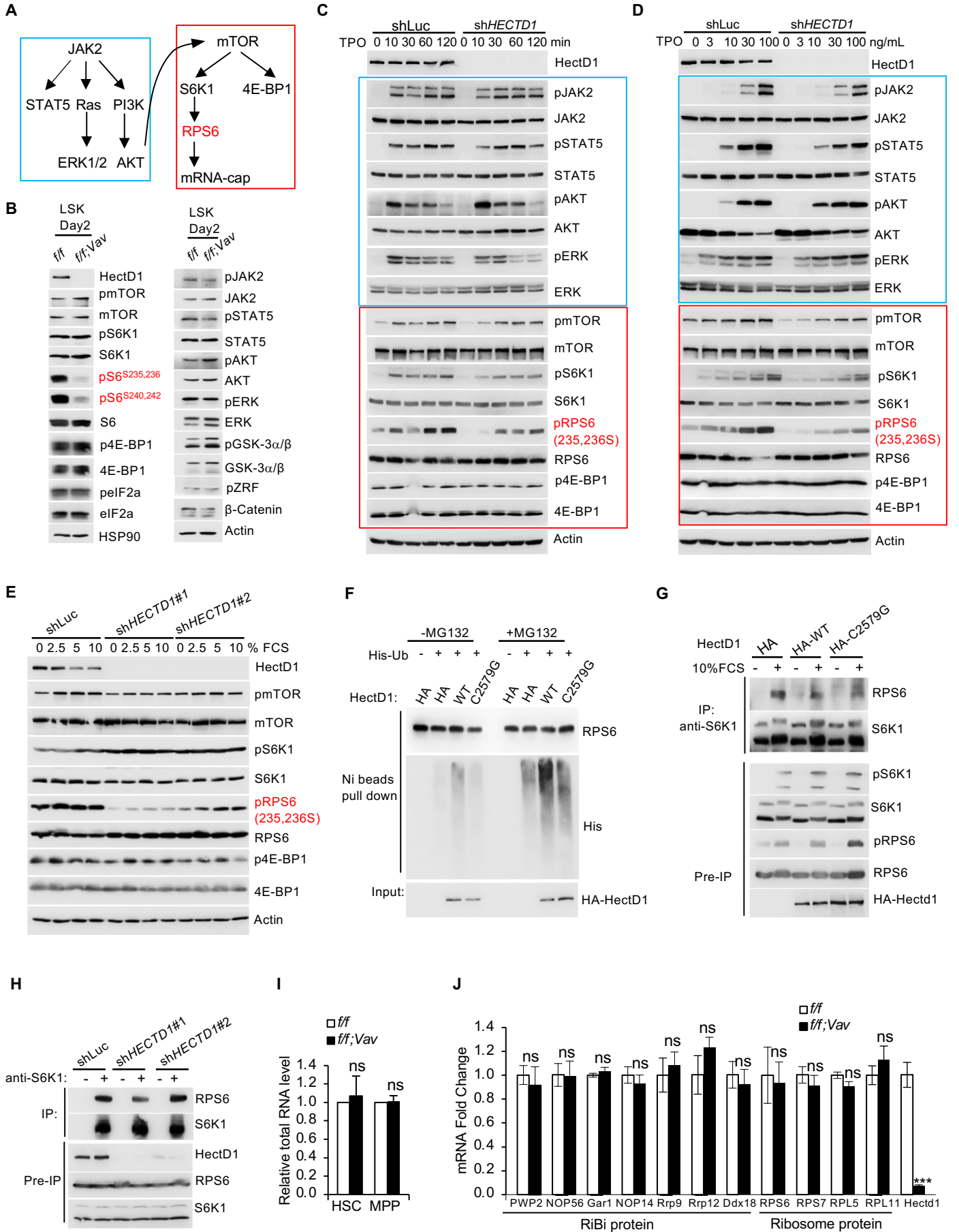


Figure S4. *Hectd1* deficiency decreases RPS6 phosphorylation independent of the mTOR pathway. Related to figure 3.

(A-B) *Hectd1* deficiency decreases RPS6 phosphorylation in 2 day-cultured LSK cells.

(A) A diagram showing different signaling pathways that we examined in LSKs and TF-1 cells.

(B) Two-day cultured LSKs from *Hectd1*^{ff} and *Hectd1*^{ff;Vav} mice were used to examine various signaling molecules in the mTOR pathway, pEIF2a, and JAK/STAT, PI3K-AKT, MAPK pathways by WB.

(C-E) *HECTD1* depletion in TF-1 cells recapitulates the signaling properties observed in *Hectd1*-deficient LSK cells.

(C-D) Signal kinetics (C) and sensitivity to cytokines (D) of JAK-STAT, PI3K-AKT, RAS-ERK and mTOR pathways were compared in shLuc and sh*HECTD1* TF-1/MPL cells stimulated with hTPO.

(E) Activation of the mTOR pathway was compared in shLuc vs sh*HECTD1* cells upon stimulation of a graded concentration of fetal calf serum (FCS). Phospho-RPS6 (pRPS6) are highlighted in red.

(F-J) HectD1 does not affect RPS6 ubiquitination, S6K1-RPS6 interaction or the transcription of RiBi genes.

(F) 293T cells were transfected with constructs expressing HA control or HA-tagged HectD1 WT or HectdD1 E3-dead mutant C2579G. 48hrs later, cells were treated with or without proteasome inhibitor MG132 for 2hr, followed by His-Ub pull down under denatured conditions.

(G) 293T cells transfected with HA control or HA-tagged HectD1 WT or mutant C2579G were either untreated or deprived of serum. Activation of S6K1 and RPS6 by serum is shown in the WB (Pre-IP). S6K1-RPS6 interaction was assessed by S6K1 immunoprecipitation (IP) followed by WB with anti-RPS6 antibodies.

(H) *HectD1* depletion does not affect S6K1-RPS6 interaction as determined by IP/WB in TF-1 cells.

(I) Total RNA was extracted and compared in HSCs and MPPs of *Hectd1*^{ff} and *Hectd1*^{ff;Vav} mice.

(J) qRT-PCR analysis of the gene expression of RiBi proteins and ribosome proteins in HSCs of *Hectd1*^{ff} and *Hectd1*^{ff;Vav} mice. n=3 in each group.

A

GO cellular component	# identified/ in category	Fold enrichment	P-value	FDR
DNA replication factor C complex (GO:0005663)	2/5	> 100	3.18E-04	1.49E-02
3M complex (GO:1990393)	2/5	> 100	3.18E-04	1.45E-02
paraspeckles (GO:0042382)	2/6	84.32	4.22E-04	1.77E-02
proteasome regulatory particle, lid subcomplex (GO:0008541)	2/8	63.24	6.75E-04	2.47E-02
chaperonin-containing T-complex (GO:0005832)	2/11	45.99	1.16E-03	3.77E-02
eukaryotic translation initiation factor 4F complex (GO:0016281)	2/13	38.92	1.56E-03	4.75E-02
exocyst (GO:0000145)	3/20	37.94	9.85E-05	6.01E-03
proteasome regulatory particle (GO:0005838)	3/22	34.5	1.27E-04	7.53E-03
proteasome accessory complex (GO:0022624)	3/25	30.36	1.80E-04	9.77E-03
Flemming body (GO:0090543)	3/31	24.48	3.23E-04	1.44E-02
cytosolic small ribosomal subunit (GO:0022627)	4/47	21.53	4.85E-05	3.25E-03
cytoplasmic stress granule (GO:0010494)	5/68	18.6	1.02E-05	8.56E-04
mitochondrial nucleoid (GO:0042645)	3/44	17.25	8.42E-04	2.97E-02
nucleoid (GO:0009295)	3/44	17.25	8.42E-04	2.92E-02
polysome (GO:0005844)	5/75	16.86	1.60E-05	1.24E-03
proteasome complex (GO:0000502)	4/66	15.33	1.68E-04	9.67E-03
endopeptidase complex (GO:0015936)	4/67	15.1	1.78E-04	9.93E-03
ficolin-1-rich granule (GO:0101002)	7/124	14.28	8.54E-07	2.15E-04
ficolin-1-rich granule lumen (GO:1904813)	7/4/124	14.28	8.54E-07	1.91E-04
small ribosomal subunit (GO:0015935)	4/79	12.81	3.24E-04	1.42E-02
cytosolic ribosome (GO:0022626)	5/111	11.39	9.54E-05	6.00E-03
growth cone (GO:0030426)	8/187	10.82	1.01E-06	1.85E-04
peptidase complex (GO:1905368)	4/94	10.76	6.09E-04	2.41E-02
site of polarized growth (GO:0030427)	8/195	10.38	1.37E-06	2.30E-04
midbody (GO:0030496)	7/182	9.73	9.74E-06	8.52E-04
nuclear matrix (GO:0016363)	4/108	9.37	1.00E-03	3.37E-02
ribosome (GO:0005840)	8/247	8.19	7.41E-06	6.78E-04
cytoplasmic ribonucleoprotein granule (GO:0036464)	7/224	7.91	3.55E-05	2.55E-03
ribonucleoprotein granule (GO:0035770)	7/235	7.54	4.77E-05	3.31E-03
secretory granule lumen (GO:0034774)	9/320	7.11	5.88E-06	7.39E-04
cytoplasmic vesicle lumen (GO:0060205)	9/324	7.03	6.48E-06	6.52E-04
vesicle lumen (GO:0031983)	9/326	6.98	6.80E-06	6.52E-04
distal axon (GO:0150034)	8/307	6.59	3.39E-05	2.53E-03
ribonucleoprotein complex (GO:1990904)	18/709	6.42	3.54E-10	1.78E-07
ribosomal subunit (GO:0044391)	5/197	6.42	1.22E-03	3.83E-02

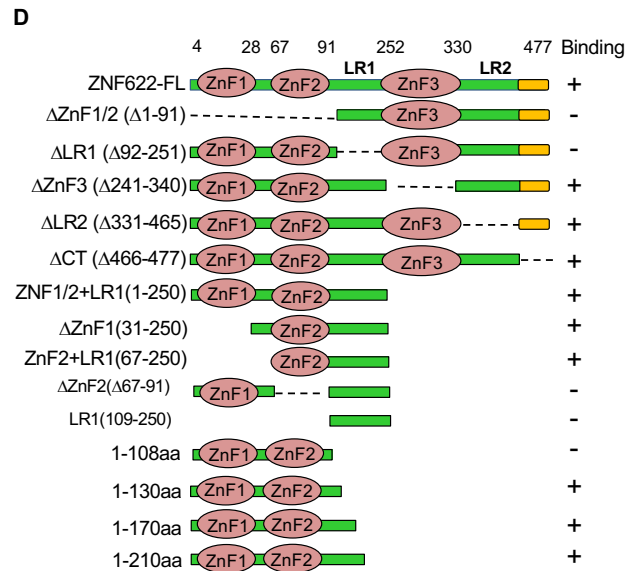
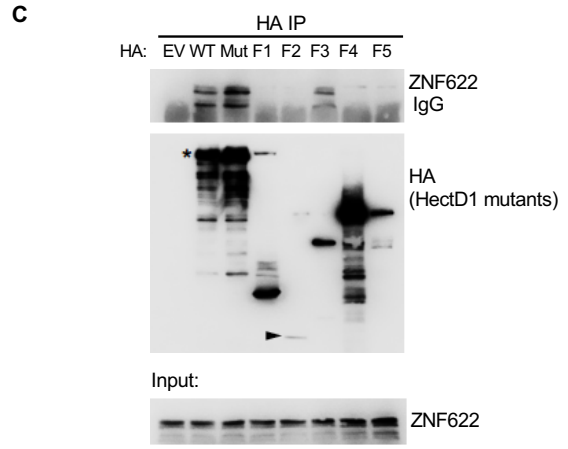
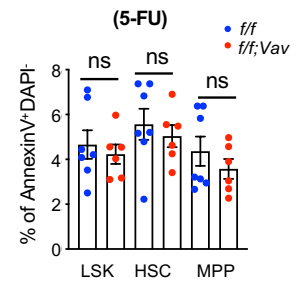
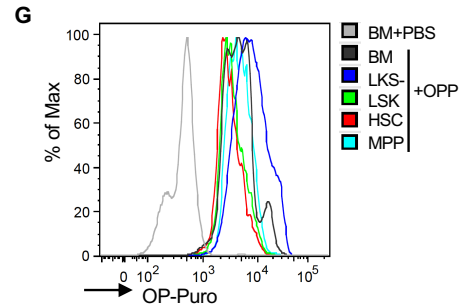
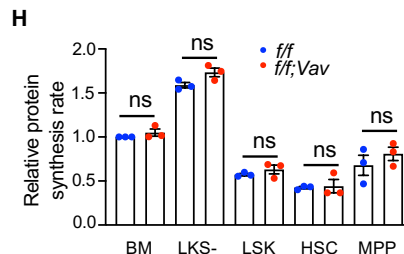
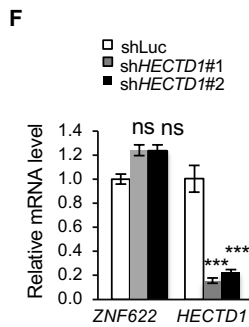
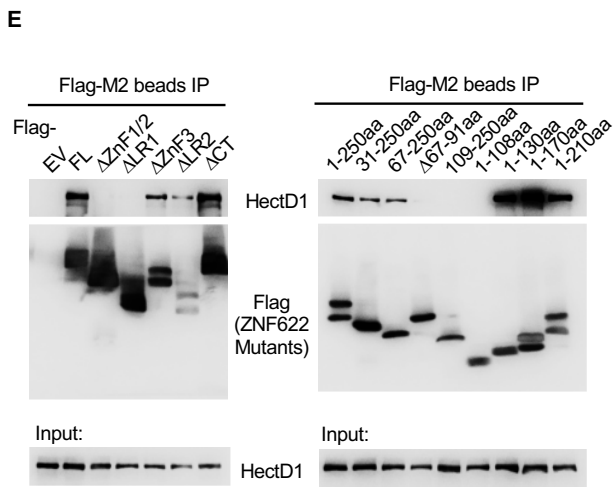
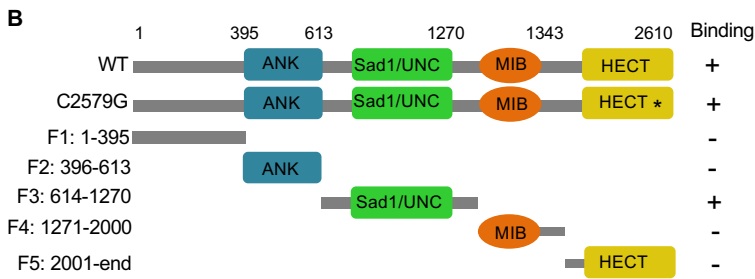


Figure S5. Panels S5A-S5F are related to figure 3. Panels S5G-S5I, related to figure 4.

(A) Gene Ontology (GO) cellular component analysis of HectD1 interactors identified in three biological replicates of HA-HectD1 immunoprecipitation/mass spectrometry (IP/MS). GO categories with fold enrichment >5 and FDR cutoff of 5% are shown.

(B-E) Mapping the interacting domains/regions of HectD1 and ZNF622 by IP/WB.

(B) Schematic demonstration of HectD1 WT, E3-dead mutant (C2579G) and deletion mutants (Fragment1-5). Positive interaction is labeled with “+”; no interaction “-”.

(C) HA-IP/WB in 293T cells transfected with HA-tagged HectD1 WT or indicated mutants. Endogenous ZNF622 was immunoblotted. The full-length HectD1 band was marked by asterisk. Fragment 2 (F2) encompassing amino acid 396-613 was lowly expressed and marked by a solid arrow.

(D) Schematic demonstration of full-length ZNF622 and its deletion mutants. Positive interaction is labeled with “+”; no interaction “-”.

(D) Flag-IP/WB in 293T cells transfected with Flag-tagged ZNF622 FL or indicated truncates/mutants. Endogenous HectD1 was immunoblotted.

(F) qRT-PCR analysis of the mRNA level of *ZNF622* in TF-1 cells with shLuc or sh*HECTD1*#1 and #2. n=3 in each group. Data are represented by mean ± SD. ns, not significant; ***: p < 0.001, as determined by unpaired two-tailed Student's *t*-tests.

(G-I) Both protein synthesis rate and cell apoptosis are not changed in primary *Hectd1*^{ff;Vav} mice.

(A) Representative histogram of OP-Puro intensity in unfractionated BM cells and different subpopulations of stem and progenitor cells of a control mouse.

(B) Quantification of relative protein synthesis rate in unfractionated BM cells and different subpopulations of stem and progenitor cells of *Hectd1*^{ff} (n=3) and *Hectd1*^{ff;Vav} (n=3) mice.

(C) Cell apoptosis analysis of LSKs, HSCs and MPPs in 5-FU challenged *Hectd1*^{ff} (n=7) and *Hectd1*^{ff;Vav} (n=6) mice by AnnexinV staining. Each symbol represents an individual mouse; bars indicate mean values; error bars indicate SE. ns: not significant, p>0.05; as determined by two-tailed Student's *t*-tests.

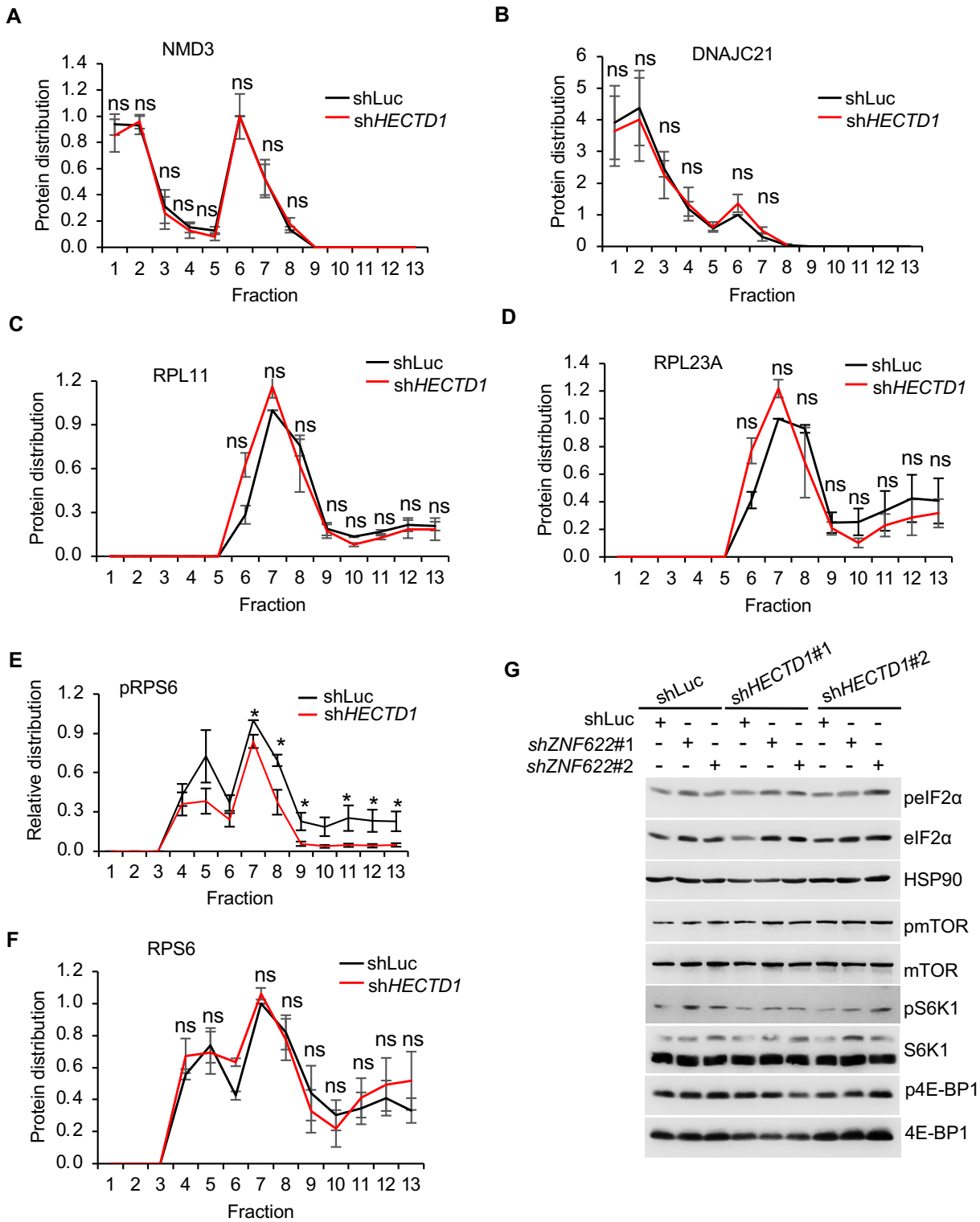


Figure S6. *HECTD1* depletion reduces phospho-RPS6, but not NMD3 or select RPLs in ribosome fractions. Panels S6A-S6F are related to figure 5; S6G, related to figure 6.

(A-F) Quantification of the relative distribution of indicated proteins in three independent polysome profiling assays of shLuc and sh*HECTD1* TF-1 cells. Data are represented by mean \pm SE. *: $p < 0.05$; ns, not significant, as determined by unpaired two-tailed Student's *t*-tests.

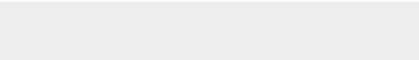
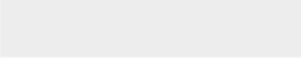
(G) **Knockdown of *ZNF622* does not change the phosphorylation of eIF2 α or mTOR activation.** WB of indicated proteins in TF-1 cells with single or double knockdown of *HECTD1* and *ZNF622*.



Click here to access/download

Supplemental Videos and Spreadsheets

Tabel S1. HectD1 interactors by IP-MS. Related to
Figure 3.xlsx





Click here to access/download

Supplemental Videos and Spreadsheets

Table S2. Primers used are shown. Related to Star
Methods.xlsx